LETTER

doi:10.1038/nature18935

CD47–blocking antibodies restore phagocytosis and prevent atherosclerosis

Yoko Kojima[1], Jens-Peter Volkmer[2], Kelly McKenna[2], Mete Civelek[3], Aldons Jake Lusis[3], Clint L. Miller[4], Daniel Direnzo[1], Vivek Nanda[1], Jianqin Ye[1], Andrew J. Connolly[5], Eric E. Schadt[6], Thomas Quertermous[4], Paola Betancur[2], Lars Maegdefessel[7], Ljubica Perisic Matic[8], Ulf Hedin[8], Irving L. Weissman[2] & Nicholas J. Leeper[1,4]

Atherosclerosis is the disease process that underlies heart attack and stroke[1]. Advanced lesions at risk of rupture are characterized by the pathological accumulation of diseased vascular cells and apoptotic cellular debris[2]. Why these cells are not cleared remains unknown[3]. Here we show that atherogenesis is associated with upregulation of CD47, a key anti-phagocytic molecule that is known to render malignant cells resistant to programmed cell removal, or 'efferocytosis'[4–7]. We find that administration of CD47-blocking antibodies reverses this defect in efferocytosis, normalizes the clearance of diseased vascular tissue, and ameliorates atherosclerosis in multiple mouse models. Mechanistic studies implicate the pro-atherosclerotic factor TNF-α as a fundamental driver of impaired programmed cell removal, explaining why this process is compromised in vascular disease. Similar to recent observations in cancer[5], impaired efferocytosis appears to play a pathogenic role in cardiovascular disease, but is not a fixed defect and may represent a novel therapeutic target.

Each day the human body turns over more than 100 billion cells[8]. To prevent the inflammatory consequences associated with the accumulation of apoptotic debris[9], these cells are rapidly and efficiently cleared through a phagocytic process known as programmed cell removal, or 'efferocytosis'[10]. Programmed cell removal is mediated by macrophages detecting phagocytic 'eat me' signals on the target cell surface, and can be countermanded by cell-surface expression of anti-phagocytic 'don't eat me' signals such as expression of CD47 (ref. 6). Whereas programmed cell removal is highly conserved across almost all physiological conditions and in all tissues, it appears to be significantly impaired in atherosclerotic cardiovascular disease[2], the leading cause of death worldwide[11]. Atherosclerosis is characterized by the accumulation of diseased macrophages and vascular smooth muscle cells (SMCs), which not only encroach on the lumen of the associated vessel but may also undergo programmed cell death[1,12]. The impaired clearance of these diseased cells by lesional macrophages is thought to explain why these cells are frequently observed in the atherosclerotic necrotic core, and may potentiate vascular inflammation and risk for eventual plaque rupture[3,13,14]. However, the mechanism underlying this defect has not yet been identified.

We recently found that the key anti-phagocytic molecule, CD47, is paradoxically upregulated by a variety of cancers[5,7,15]. This renders malignant cells resistant to classic immune surveillance machinery

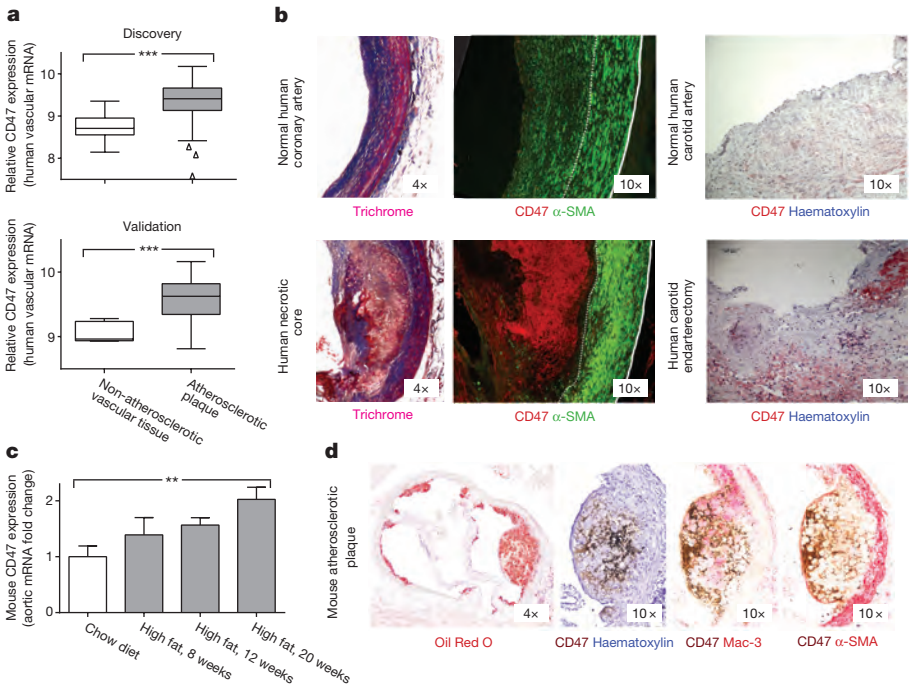

Figure 1 | CD47 is upregulated in atherosclerosis. a, Microarray expression profiling in two carotid endarterectomy cohorts reveals that CD47 expression is significantly increased in human atherosclerotic plaque, relative to non-diseased vascular tissue (data displayed as Tukey box plots, $n = 182$ subjects). **b**, Immunostaining identifies intense CD47 upregulation within the necrotic core of human atherosclerotic coronary artery lesions (left) and carotid plaques (right). **c**, TaqMan mRNA analysis confirms that vascular CD47 expression progressively increases in a mouse model of atherosclerosis ($apoE^{-/-}$ mice fed high-fat diet, grey), relative to control animals (C57BL/6 mice fed chow, white, $n = 4$ mice per time point). **d**, Immunohistochemistry staining with a biotin-labelled antibody (brown) reveals that CD47 expression co-localizes with apoptotic tissue in murine atherosclerotic plaque. $^{***}P < 0.001$, $^{**}P$ for trend < 0.03. Error bars represent the standard error of the mean (s.e.m.).

[1]Department of Surgery, Division of Vascular Surgery, Stanford University School of Medicine, Stanford, California 94305, USA. [2]Institute for Stem Cell Biology and Regenerative Medicine, Stanford University School of Medicine, Stanford, California 94305, USA. [3]Department of Medicine, David Geffen School of Medicine, University of California, Los Angeles, Los Angeles, California 90095, USA. [4]Department of Medicine, Division of Cardiovascular Medicine, Stanford University School of Medicine, Stanford, California 94305, USA. [5]Department of Pathology, Stanford University School of Medicine, Stanford, California 94305, USA. [6]Department of Genetics and Genomic Sciences, Mount Sinai School of Medicine, New York, New York 10029, USA. [7]Department of Medicine, Karolinska Institute, Stockholm, Sweden. [8]Department of Molecular Medicine and Surgery, Karolinska Institute, Stockholm, Sweden.

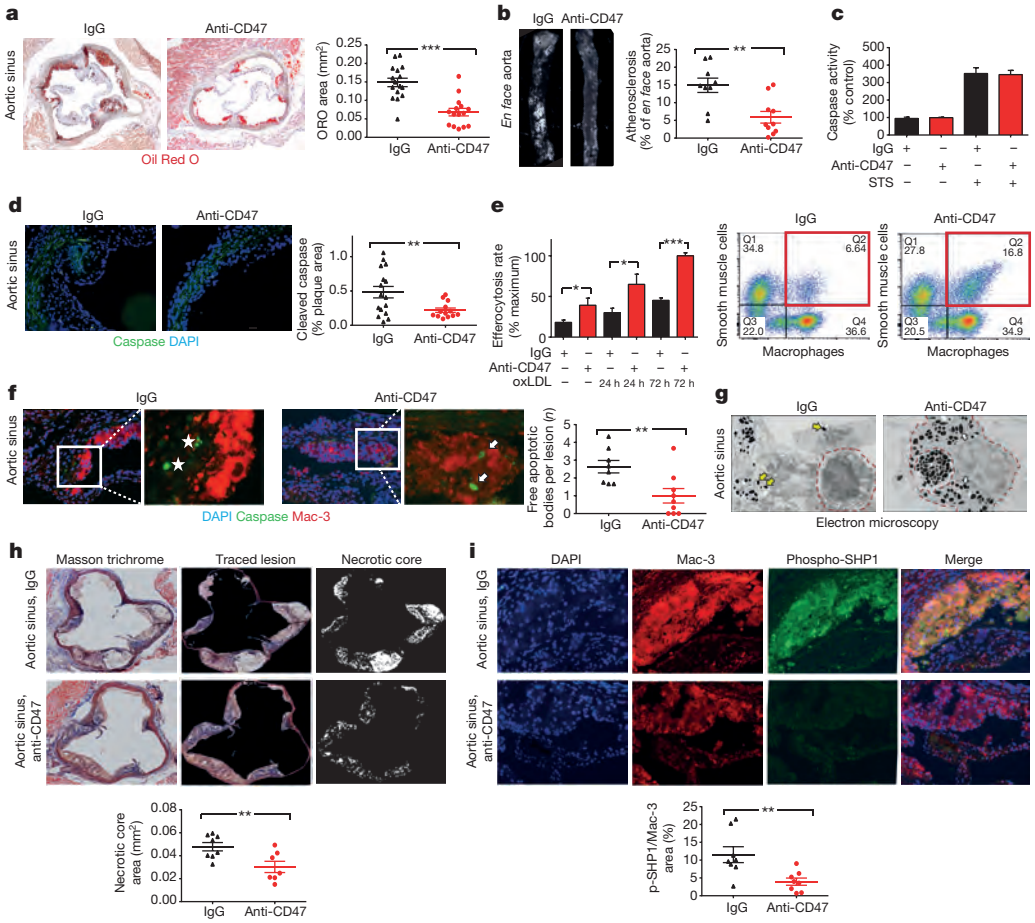

Figure 2 | Inhibition of CD47 stimulates efferocytosis and prevents atherosclerosis. a, Compared to mice treated with control antibodies (IgG, $n = 16$), mice treated with inhibitory anti-CD47 antibodies ($n = 15$) develop significantly smaller atherosclerotic plaques, as measured by Oil Red O (ORO) content in the aortic sinus. **b**, Total aortic atherosclerosis content is also reduced. **c**, **d**, Inhibition of CD47 signalling does not alter the rate of programmed cell death *in vitro* (**c**), but does reduce the accumulation of apoptotic bodies *in vivo* (**d**). **e**, Anti-CD47 antibody promotes efferocytosis of vascular cells at baseline and after exposure to pro-atherosclerotic lipids. Representative FACS phagocytosis plots for lipid-loaded (72 h) SMCs shown on the right (all assays repeated in triplicate). **f**, *In vivo* anti-CD47 antibody reduces the number of 'free' apoptotic bodies not associated with phagocytic macrophages, potentially indicative of increased efferocytosis (stars indicate 'free' apoptotic bodies, arrows indicate 'not-free' apoptotic bodies). **g**, Electron microscopy confirms that mice treated with anti-CD47 antibodies display features of enhanced intraplaque efferocytosis, including an increased prevalence of macrophages which had ingested multiple apoptotic bodies (white arrows) and a reduced burden of 'free' apoptotic bodies (yellow arrows). **h**, Mice treated with anti-CD47 antibodies develop smaller necrotic cores than mice treated with IgG. **i**, Anti-CD47 antibody inhibits phosphorylation of lesional SHP1, a key anti-phagocytic effector molecule known to signal downstream of CD47. STS, staurosporine. Comparisons made by two-tailed *t*-tests. $***P < 0.001$, $**P < 0.01$, $*P < 0.05$. Error bars represent s.e.m.

such as the tumoricidal macrophage, and is now recognized as a fundamental driver of tumour growth. To determine if dysregulated CD47 may also contribute to atherogenesis, we evaluated its expression in two independent human vascular tissue biobanks[16,17]. We found that CD47 is consistently upregulated in human atherosclerotic plaque compared to non-atherosclerotic vascular tissue (Fig. 1a), and in subjects with symptomatic cerebrovascular disease (stroke or transient ischaemic attack) compared to those with stable asymptomatic lesions (Extended Data Fig. 1a). Because some efferocytosis molecules are known to undergo post-translational modification[18], we also performed immunofluorescence and immunohistochemical staining of human coronary and carotid arteries, which confirmed that CD47 is progressively upregulated during atherogenesis and appears to localize intensely to the necrotic core (Fig. 1b, Extended Data Fig. 1b–g). Similar findings were observed in mouse models of atherosclerosis and other publically available microarray data sets (Fig. 1c, d, Extended Data Fig. 2). Together, these data suggest that pathologic upregulation of 'don't eat me' molecules may explain why phagocytosis is impaired within the human atherosclerotic plaque, which may promote lesion expansion over time.

To determine if this defect could be exploited as a translational target for cardiovascular disease, we treated a cohort of atheroprone animals (apolipoprotein-E-deficient ($apoE^{-/-}$) mice implanted with angiotensin-II-infusing minipumps[19]) with an inhibitory antibody directed against CD47 (Extended Data Fig. 3a)[15]. Compared to IgG control, anti-CD47 antibody treatment was associated with a marked reduction in atherosclerosis, both in the aortic sinus and *en face* in the aorta (Fig. 2a, b, Extended Data Fig. 3b, c). Similar results were observed in several additional models, including models of chronic atherosclerosis, plaque vulnerability and in mice with established lesions, as would be encountered clinically (Extended Data Fig. 3d–h). Although anti-CD47 antibodies had no effect on apoptosis *in vitro* (Fig. 2c, Extended Data Fig. 4a, b), we observed significantly fewer apoptotic bodies in the lesions of anti-CD47-treated animals *in vivo* (Fig. 2d). To reconcile this discrepancy, we used an established *in vitro* phagocytosis assay, and found that anti-CD47 antibodies potently induced the clearance of diseased and apoptotic vascular SMCs and macrophages that had been exposed to oxidized phospholipids to simulate the atherosclerotic environment (Fig. 2e, Extended Data Fig. 4c–f). Similarly, the number of 'free' apoptotic

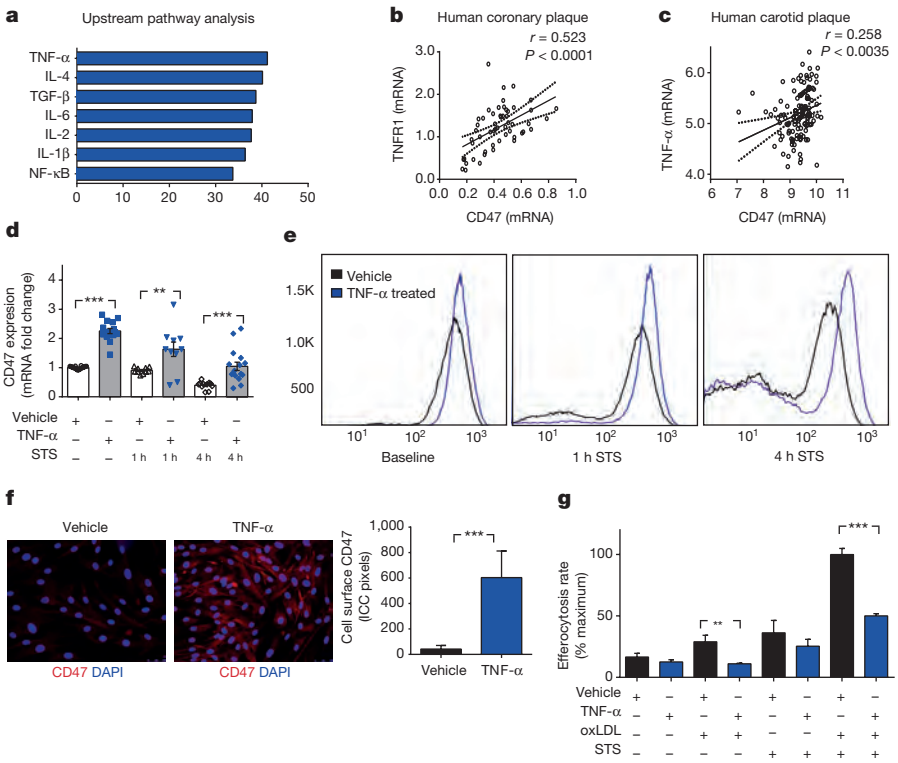

Figure 3 | The pro-atherosclerotic cytokine TNF-α induces CD47 expression and renders vascular cells resistant to phagocytic clearance. **a**, Ingenuity Pathway Analysis identifies TNF-α as the regulator most likely to be upstream of genes that are co-expressed with CD47 in vascular tissue *ex vivo*. **b**, **c**, Co-expression studies confirm that CD47 is positively correlated with the canonical TNF-α receptor, TNFR1, in human coronary plaque (**b**) and TNF-α levels in human carotid plaque (**c**). The Pearson correlation coefficient was determined assuming a Gaussian distribution and *P* values were determined using a two-tailed test shown with the 95% confidence band of the best fit line. **d**, *In vitro*, TNF-α treatment significantly increases the basal expression of CD47 in vascular SMCs, and blunts the decrease expected to occur during apoptosis. **e**, **f**, Flow cytometry (**e**) and fluorescent microscopy (**f**) confirm that TNF-α increases the cell-surface expression of CD47 on vascular cells at baseline and during programmed cell death. ICC, immunocytochemistry. **g**, *In vitro* efferocytosis assays indicate that TNF-α treatment renders vascular SMCs resistant to programmed cell clearance under a variety of pro-atherosclerotic conditions. Comparisons made by two-tailed *t*-tests. $***P < 0.001$, $**P < 0.01$. Error bars represent s.e.m.

bodies not associated with an intraplaque macrophage (indicative of failed efferocytosis) was reduced after anti-CD47 antibody treatment *in vivo*, as suggested by co-localization studies (Fig. 2f, Extended Data Fig. 5a) and electron microscopy (Fig. 2g, Extended Data Fig. 5b). Ultimately, these animals accumulated less apoptotic debris and developed lesions with smaller necrotic cores (Fig. 2h, Extended Data Fig. 5c). From a mechanistic perspective, anti-CD47 antibody therapy was associated with a marked suppression of intraplaque SHP1 phosphorylation, confirming interruption of the anti-phagocytic signalling axis downstream of SIRPα, the cognate anti-phagocytic receptor of CD47 (Fig. 2i, Extended Data Fig. 5d). These findings indicate that targeting CD47 can reduce atherosclerosis, and appears to do so by specifically reactivating efferocytosis within the lesion, without altering programmed cell death itself.

In addition to regulating phagocytosis, CD47 is also known to serve as a receptor for the vasoactive and nitric-oxide-regulating cytokine thrombospondin-1 (TSP1)[20]. However, mice treated with anti-CD47 antibodies and IgG control had similar systemic blood pressures (Extended Data Fig. 6a) and rates of pulmonary nitric oxide elaboration (Griess reaction, Extended Data Fig. 6b), suggesting that anti-CD47 antibodies did not alter endothelial function *in vivo*. Further, anti-CD47 antibodies did not influence TSP1 signalling *in vitro*, having no modifying effect on TSP1-dependent MAPK signalling, eNOS phosphorylation, SMC proliferation or phagocytosis rates (Extended Data Fig. 6c–f). These data suggest that the anti-CD47 antibodies used in this study mediated anti-atherosclerotic effects independently of TSP1 signalling. Although full-dose anti-CD47 antibody therapy was again found to promote splenic erythrophagocytosis and compensatory reticulocytosis (CD47 is a critical marker of self that is downregulated on ageing red blood cells)[4,15], this toxicity was self-limited and anaemia was not observed with chronic administration. Otherwise, this pro-efferocytic agent appeared to be well-tolerated, having no discernible effect on circulating leukocytes, lipid levels, or other metabolic parameters relevant to vascular disease (Extended Data Fig. 6g–u and Extended Data Table 1a).

To investigate why CD47 is upregulated in atherosclerosis, we used a bioinformatic approach in which we tested for genetic co-expression across panels of mouse and human vascular tissue. This yielded a list of genes that were significantly co-expressed with CD47 *in vivo* (Extended Data Fig. 7a). Pathway analyses of these genome-wide data sets identified 'inflammation mediated by chemokine and cytokine signaling pathway' as the top pathway associated with CD47 in vascular tissue (Extended Data Fig. 7b and Extended Data Table 1b, c), and specifically implicated TNF-α as the factor most likely to function as its upstream regulator (Fig. 3a). Subsequent correlation studies identified a strong positive association between CD47 and both the canonical TNF receptor, TNFR1 (Fig. 3b), as well as TNF-α itself (Fig. 3c), in human atherosclerotic vessel specimens. Similarly, CD47 expression levels were correlated with TNF-α levels in tissue from atherosclerotic mice and confirmatory human data sets (Extended Data Fig. 7c, d). Together, these informatics and co-expression studies implicate TNF-α—a proinflammatory cytokine known to be upregulated in atherosclerosis—in CD47-dependent vascular disease[21,22].

To investigate the causality of these associations, we next tested whether CD47 is directly downstream of TNF-α. We found that treatment of vascular SMCs with recombinant TNF-α led to a

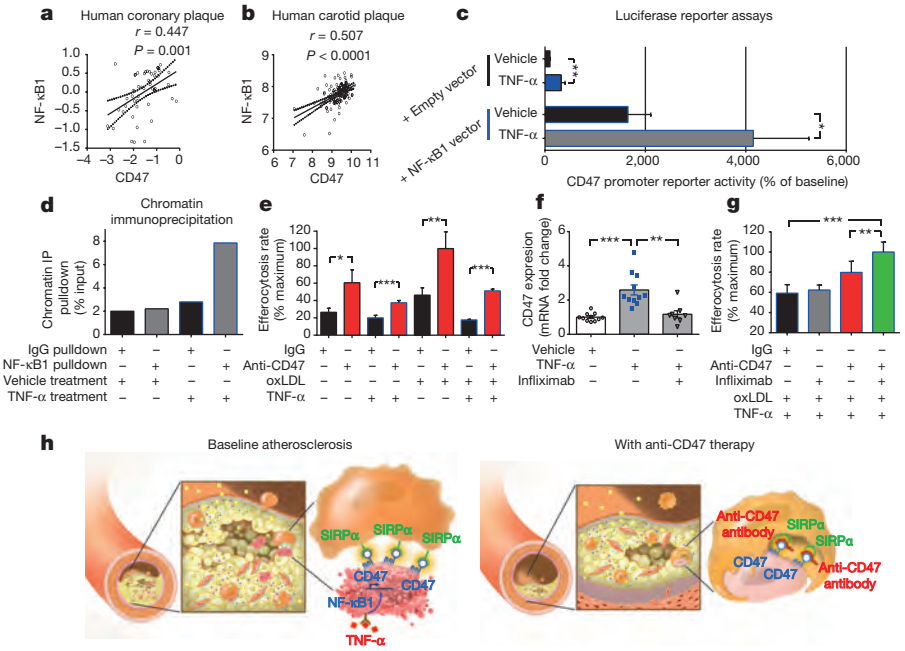

Figure 4 | TNF-α promotes CD47 expression via NF-κB1 and is a translational cardiovascular target. a, **b**, Co-expression analyses confirm that NF-κB1 is significantly correlated with CD47 expression in both human coronary (**a**) and carotid (**b**) atherosclerotic plaque. Pearson correlation coefficients were determined assuming a Gaussian distribution and *P* values were determined using a two-tailed test. **c**, Dual luciferase reporter assays reveal that *CD47* promoter activity is stimulated in cells treated with TNF-α (top), but that this effect is significantly enhanced in cells co-transfected with an NF-κB1 expression vector. **d**, Chromatin immunoprecipitation studies confirm significant enrichment of NF-κB1 protein on the *CD47* promoter in TNF-α-treated human coronary artery SMCs. **e**, *In vitro* efferocytosis assays reveal that anti-CD47 antibody enhances the clearance of cells exposed to TNF-α, and that its pro-efferocytic capacity is enhanced under pro-atherosclerotic conditions. **f**, Pretreatment with the anti-TNF-α monoclonal antibody infliximab prevents the upregulation in *Cd47* mRNA that normally occurs in SMCs exposed to TNF-α. **g**, Concomitant inhibition of CD47 and TNF-α using anti-CD47 antibodies and infliximab, respectively, produces synergistic benefit in the clearance of diseased vascular cells, as assessed by ANOVA. **h**, Putative mechanism explaining why efferocytosis is impaired in cardiovascular disease, and how inhibition of CD47-SIRPα signalling could represent a new therapeutic target. Comparisons made by two-tailed *t*-tests, unless otherwise specified. $***P < 0.001$, $**P < 0.01$, $*P < 0.05$. Error bars represent s.e.m.

consistent upregulation of cellular CD47 expression, whereas no effect was observed with a variety of other common pro-atherosclerotic or proinflammatory insults (Extended Data Fig. 7e–h). Further, TNF-α blunted the progressive decrease in CD47 expression normally expected to occur during programmed cell death (Fig. 3d–f, Extended Data Fig. 7i–l). As a result of their higher levels of anti-phagocytic molecules, TNF-α-treated cells were less likely to be phagocytosed by macrophages, particularly when concomitantly exposed to oxidized low-density lipoproteins (oxLDL) and pro-apoptotic stimuli (Fig. 3g, Extended Data Fig. 7m). Because impaired efferocytosis is known to incite proinflammatory cytokine elaboration[9], it is possible that a positive feedback loop underlies the co-localization of TNF-α, CD47, and uncleared pathological cells and apoptotic bodies within the atherosclerotic plaque[22].

Analysis of the *CD47* promoter in vascular SMCs revealed a region of open chromatin predicted to contain binding sites for several of the NF-κB transcription factors known to be downstream of TNFR1 (Extended Data Fig. 8a and Extended Data Table 1d). Among these, the classical proinflammatory factor NF-κB1 (p50) was found to be positively correlated with CD47 expression in both human coronary and carotid plaques (Fig. 4a, b, Extended Data Fig. 8b). Luciferase reporter assays performed with a vector containing the *CD47* promoter revealed that TNF-α treatment stimulated basal CD47 expression, and that the effect was specifically enhanced when NF-κB1was simultaneously overexpressed in these cells (Fig. 4c, Extended Data Fig. 8c–e). Chromatin immunoprecipitation assays confirmed that NF-κB1 binds to the *CD47* promoter *in vitro*, and that this occupancy is increased several fold upon treatment with TNF-α (Fig. 4d, Extended Data Fig. 8f).

From a translational perspective, we found that anti-CD47 antibodies were able to stimulate efferocytosis in TNF-α-treated cells, and that the effect was most pronounced under dyslipidaemic, pro-atherosclerotic conditions (Fig. 4e). A modest incremental benefit was observed when anti-CD47 antibody therapy was combined with commercially available anti-TNF-α therapies, such as infliximab or etanercept, probably because of their inhibitory influence on CD47 expression in mouse and human tissue (Fig. 4f, g, Extended Data Fig. 9). These data are particularly provocative given the observation that patients prescribed TNF-α-inhibiting antibodies for inflammatory disorders such as lupus and rheumatoid arthritis appear to be protected from myocardial infarction[21,23].

The finding that CD47 expression is pathologically upregulated in both cancer and cardiovascular disease suggests a commonality between these two conditions. In leukaemogenesis, cancer stem cells out-compete normal haematopoietic stem cells, while countering signalling associated with programmed cell removal; viable myelodysplastic syndrome haematopoietic oligolineage progenitors express the phagocytic signal calreticulin, but not CD47, whereas acute myeloid leukaemia derived from myelodysplastic syndromes are positive for CD47 expression[24]. Similar cellular processes in the vasculature may explain the recent observations that de-differentiated SMCs undergo clonal expansion within the atherosclerotic plaque[25,26]. Furthermore, the top cardiovascular locus identified by genome-wide association studies surprisingly resides near an important tumour suppressor locus[27], which in turn regulates SMC efferocytosis[17]. Future studies will need to examine whether expansion of $CD47^{hi}$ SMC clones contributes to atherosclerosis, and if their clearance can be accomplished without the induction of anaemia (for example, with a dose-escalation approach that appears to be safe in non-human primates[28] and is currently being pursued in first-in-human clinical trials[29]).

Together, these data provide insights into why programmed cell removal is impaired in the atherosclerotic plaque, and how this may

promote lesion expansion. Our findings bolster the 'inflammatory hypothesis' of atherosclerosis[30], and specifically link cytokine signalling with anti-phagocytic signalling in vascular disease. Given the experimental success of pro-efferocytic therapies in the oncology field using antibodies that block the CD47 signal[5], it is possible that these findings will provide a novel nonsurgical treatment of cardiovascular disease (mechanism shown in Fig. 4h).

Online Content Methods, along with any additional Extended Data display items and Source Data, are available in the online version of the paper; references unique to these sections appear only in the online paper.

Received 8 March; accepted 16 June 2016.
Published online 20 July 2016.

1. Libby, P., Ridker, P. M. & Hansson, G. K. Progress and challenges in translating the biology of atherosclerosis. *Nature* **473,** 317–325 (2011).
2. Schrijvers, D. M., De Meyer, G. R., Kockx, M. M., Herman, A. G. & Martinet, W. Phagocytosis of apoptotic cells by macrophages is impaired in atherosclerosis. *Arterioscler. Thromb. Vasc. Biol.* **25,** 1256–1261 (2005).
3. Thorp, E. & Tabas, I. Mechanisms and consequences of efferocytosis in advanced atherosclerosis. *J. Leukoc. Biol.* **86,** 1089–1095 (2009).
4. Oldenborg, P. A. *et al.* Role of CD47 as a marker of self on red blood cells. *Science* **288,** 2051–2054 (2000).
5. Chao, M. P., Majeti, R. & Weissman, I. L. Programmed cell removal: a new obstacle in the road to developing cancer. *Nat. Rev. Cancer* **12,** 58–67 (2011).
6. Gardai, S. J. *et al.* Cell-surface calreticulin initiates clearance of viable or apoptotic cells through trans-activation of LRP on the phagocyte. *Cell* **123,** 321–334 (2005).
7. Majeti, R. *et al.* CD47 is an adverse prognostic factor and therapeutic antibody target on human acute myeloid leukemia stem cells. *Cell* **138,** 286–299 (2009).
8. Kinchen, J. M. & Ravichandran, K. S. Phagocytic signaling: you can touch, but you can't eat. *Curr. Biol.* **18,** R521–R524 (2008).
9. Fadok, V. A. *et al.* Macrophages that have ingested apoptotic cells *in vitro* inhibit proinflammatory cytokine production through autocrine/paracrine mechanisms involving TGF-β, PGE2, and PAF. *J. Clin. Invest.* **101,** 890–898 (1998).
10. Henson, P. M., Bratton, D. L. & Fadok, V. A. Apoptotic cell removal. *Curr. Biol.* **11,** R795–R805 (2001).
11. World Health Organization. The top ten causes of death. http://www.who.int/mediacentre/factsheets/fs310/en/ (2014).
12. Shankman, L. S. *et al.* KLF4-dependent phenotypic modulation of smooth muscle cells has a key role in atherosclerotic plaque pathogenesis. *Nat. Med.* **21,** 628–637 (2015).
13. Tabas, I. Macrophage death and defective inflammation resolution in atherosclerosis. *Nat. Rev. Immunol.* **10,** 36–46 (2010).
14. Thorp, E., Cui, D., Schrijvers, D. M., Kuriakose, G. & Tabas, I. Mertk receptor mutation reduces efferocytosis efficiency and promotes apoptotic cell accumulation and plaque necrosis in atherosclerotic lesions of apoe$^{-/-}$ mice. *Arterioscler. Thromb. Vasc. Biol.* **28,** 1421–1428 (2008).
15. Willingham, S. B. *et al.* The CD47-signal regulatory protein alpha (SIRPα) interaction is a therapeutic target for human solid tumors. *Proc. Natl Acad. Sci. USA* **109,** 6662–6667 (2012).
16. Perisic, L. *et al.* Profiling of atherosclerotic lesions by gene and tissue microarrays reveals PCSK6 as a novel protease in unstable carotid atherosclerosis. *Arterioscler. Thromb. Vasc. Biol.* **33,** 2432–2443 (2013).
17. Kojima, Y. *et al.* Cyclin-dependent kinase inhibitor 2B regulates efferocytosis and atherosclerosis. *J. Clin. Invest.* **124,** 1083–1097 (2014).
18. Garbin, U. *et al.* Expansion of necrotic core and shedding of Mertk receptor in human carotid plaques: a role for oxidized polyunsaturated fatty acids? *Cardiovasc. Res.* **97,** 125–133 (2013).
19. Daugherty, A., Manning, M. W. & Cassis, L. A. Angiotensin II promotes atherosclerotic lesions and aneurysms in apolipoprotein E-deficient mice. *J. Clin. Invest.* **105,** 1605–1612 (2000).
20. Isenberg, J. S. *et al.* CD47 is necessary for inhibition of nitric oxide-stimulated vascular cell responses by thrombospondin-1. *J. Biol. Chem.* **281,** 26069–26080 (2006).
21. Bäck, M. & Hansson, G. K. Anti-inflammatory therapies for atherosclerosis. *Nat. Rev. Cardiol.* **12,** 199–211 (2015).
22. Hopkins, P. N. Molecular biology of atherosclerosis. *Physiol. Rev.* **93,** 1317–1542 (2013).
23. Greenberg, J. D., Furer, V. & Farkouh, M. E. Cardiovascular safety of biologic therapies for the treatment of RA. *Nat. Rev. Rheumatol.* **8,** 13–21 (2011).
24. Pang, W. W. *et al.* Hematopoietic stem cell and progenitor cell mechanisms in myelodysplastic syndromes. *Proc. Natl Acad. Sci. USA* **110,** 3011–3016 (2013).
25. Feil, S. *et al.* Transdifferentiation of vascular smooth muscle cells to macrophage-like cells during atherogenesis. *Circ. Res.* **115,** 662–667 (2014).
26. Chung, I. M., Schwartz, S. M. & Murry, C. E. Clonal architecture of normal and atherosclerotic aorta: implications for atherogenesis and vascular development. *Am. J. Pathol.* **152,** 913–923 (1998).
27. McPherson, R. *et al.* A common allele on chromosome 9 associated with coronary heart disease. *Science* **316,** 1488–1491 (2007).
28. Liu, J. *et al.* Pre-clinical development of a humanized anti-CD47 antibody with anti-cancer therapeutic potential. *PLoS One* **10,** e0137345 (2015).
29. ClinicalTrials.gov: NCT02216409.
30. Libby, P. Inflammation in atherosclerosis. *Nature* **420,** 868–874 (2002).

Supplementary Information is available in the online version of the paper.

Acknowledgements This study was supported by the National Institutes of Health (R01HL12522401 and R01HL12337001 to NJL and U01HL099999 to ILW) and the Ludwig Center at Stanford. The authors wish to acknowledge J. Knowles for his critical review of the manuscript.

Author Contributions Y.K. designed and conducted most experiments including the mouse microsurgery, morphometric analyses, *in vitro* cell culture, TaqMan, western blot, ChIP and luciferase reporter experiments. V.N., D.D. and L.M. assisted with the electron microscopy studies and blinded histology. J.Y., J.P.V. and K.M. conducted the *in vitro* efferocytosis assays and FACS studies. L.P. and U.H. performed the carotid staining and BiKE biobank analyses. A.C. provided coronary samples and assisted with the histopathological studies. M.C., A.J.L., E.S., P.B., T.Q. and C.M. conducted the microarray, co-expression and *in silico* bioinformatic studies. Y.K., I.L.W. and N.J.L. conceived the study, analysed the data and wrote the paper. All authors discussed the results and commented on the manuscript.

Author Information Reprints and permissions information is available at www.nature.com/reprints. The authors declare competing financial interests: details are available in the online version of the paper. Readers are welcome to comment on the online version of the paper. Correspondence and requests for materials should be addressed to N.J.L. (nleeper@stanford.edu).

Reviewer Information *Nature* thanks I. Tabas and the other anonymous reviewer(s) for their contribution to the peer review of this work.

METHODS

Data reporting. The experiments were not randomized. The investigators were not blinded to allocation during experiments, but were blinded during data analysis and interpretation. No statistical methods were used to predetermine sample size.

Human cardiovascular tissue. *Carotid endarterectomy samples.* In this study, a total of 182 human carotid endarterectomy samples and nonatherosclerotic control arteries were used. These include heterogeneous atherosclerotic plaque samples obtained from patients undergoing surgery for symptomatic (stroke or transient ischaemic attack) or asymptomatic (no history of cerebrovascular event) high-grade carotid stenosis (>50% NASCET criteria) as part of the Biobank of Karolinska Endarterectomies (BiKE). 15 nonatherosclerotic control arteries (iliac artery and aorta) were obtained from organ donors without any history of cardiovascular disease. Patients were consecutively enrolled in the study, with the first 127 constituting the discovery cohort (40 asymptomatic, 87 symptomatic) and the next 50 constituting the validation cohort (10 asymptomatic, 40 symptomatic). All samples were collected with informed consent from patients, organ donors or their guardians. The BiKE study was approved by the Ethical Committee of the Northern Stockholm. DNA and RNA was extracted from these specimens and analysed by Ilumina 610w -QuadBead SNP-chips and the Affymetrix HG-U133 plus 2.0 microarrays (discovery cohort) or the Affymetrix HG-U133a Genechip arrays (validation cohort), as previously described[16,17] and deposited in Gene Expression Omnibus (accession number GSE21545). Robust multi-array average (RMA) normalization was performed and processed gene expression data was returned in $\log_2$-scale. The relative expression of each gene was determined by comparing the pixel intensity of the 11 probe pairs which correspond to each transcript to the 'normalization control set' specific to each array (see http://www.affymetrix.com/support/technical/technotes/expression_comparison_technote.pdf and http://www.affymetrix.com/support/technical/datasheets/hgu133arrays_datasheet.pdf). Student's *t*-test with correction for multiple comparisons according to the Sidak–Bonferroni method was used for statistical analyses of microarray data. Pearson's correlations were calculated to determine associations between expression of the gene of interest and other genes from microarrays. Publically available data from the Helsinki Carotid Endarterectomy Study (HeCES) were analysed as a second human validation cohort[31]. Additional publically available vascular and nonvascular microarray data deposited in GEO were also analysed (as indicated by GSE number in the corresponding figure legend), including studies of microdissected atherosclerotic plaques and samples taken from individuals treated with commercially available TNF-α inhibitors. A P value <0.05 was considered to indicate significance.

Coronary artery samples. In this study, a total of 114 human coronary artery samples were used. 51 atherosclerotic epicardial coronary artery segments were harvested from 22 orthotopic heart transplant donors, as previously described[32]. Additionally, 56 coronary artery segments were extracted from atherosclerotic intracoronary plaques in patients undergoing coronary atherectomy, as previously described[33]. Briefly, longitudinal atherectomy was performed with the Silverhawk atherectomy catheter in arteries with flow-limiting stenosis after diagnostic angiography. RNA was isolated from both sets of specimens and hybridized to custom dual-dye gene expression microarrays representing approximately 22,000 features[32,33]. Briefly, the custom probe set was identified from data mining and curation of atherosclerosis and vascular cell-culture-based expression analyses and combined with the Agilent Human 1A and 1B arrays. In each microarray experiment, the expression levels of CD47 were determined by array-specific hybridization probe sets (~10 per transcript). Automated feature extraction software was used to filter out background or saturated spot intensities to eliminate inherent probe and spatial biases during the fluorescent detection. This software computes the $\log_2$ ratios and filters features by P value. These values were normalized according to protocol for each array, using a locally weighted linear regression curve fit (LOWESS) to correct for dye biases. This normalization procedure results in array specific $\log_2$ ratios, and provides accurate measures of relative gene expression differences (http://www.affymetrix.com/support/technical/datasheets/human_datasheet.pdf). Normalized data from candidate transcripts were then used to calculate a Pearson correlation coefficient r assuming a Gaussian distribution, and two-tailed P values were calculated for each correlation coefficient.

In addition to samples obtained for RNA analysis, an additional seven right coronary arteries were obtained from rapid autopsies from adult patients with a spectrum of coronary artery disease for histological analysis. The arteries were fixed with 4% paraformaldehyde (PFA) for several hours, and immersed in 30% sucrose at 4 °C overnight. The coronaries were then serially sectioned and segments of atheroma and relatively normal coronary artery were embedded in paraffin or OCT, and sectioned at 7-μM thickness.

For immunohistochemical staining, paraffin slides were deparaffinized and rehydrated with xylene and alcohol gradients, and antigen retrieval was performed in sodium citrate buffer (10 mM sodium citrate, 0.05% Tween 20, pH 6.0) using a pressure cooker. The sections were blocked with 5% goat serum, and then stained with primary antibodies (anti-CD47, Abcam B6H12.2, 2 μg ml^{-1}) or mouse IgG1 kappa (eBioscience, 2 μg ml^{-1}) at 4 °C overnight. The sections were washed in TBS, incubated with MACH4 kit (Biocare Medical) according to the manufacturer's instructions, and then detected using the Vulcan Fast Red Chromogen kit2 (Biocare Medical). Staining for SMC content was accomplished by washing sections in water and PBS, followed by incubation with anti-SM22 alpha antibodies (Abcam, ab14106, 1:300). The sections were washed with PBS, incubated with Alexa Fluor 488 goat anti-Rabbit (Life technologies, 1:250), washed, and mounted with Vectashield Mounting medium with DAPI (Vector Laboratories). Pictures were taken by Nikon digital camera mounted on an inverted fluorescence microscope. Serial sections were prepared as described above, and also stained with Masson's trichrome (Richard-Allan), or haematoxylin and eosin (Richard-Allan). For the staining of frozen sections, OCT was removed in water, and the sections were stained with Oil Red O (ORO, Sigma-Aldrich, O0625, 0.5%), haematoxylin and eosin (H&E, Richard-Allan), smooth muscle alpha-actin (Abcam, ab5694, 1:300), HMGB1 (Abcam, ab18256, 1:100), CD206 (Abcam, ab64693, 1:50), CD47 (Abcam B6H12.2 or Novus Biologicals, #NBP2-31106, 1:50) or mouse IgG1 kappa (eBioscience). Secondary antibodies included Alexa Fluor 594 goat anti-mouse (Life technologies, A11005, 1:300) and Alexa Fluor 488 goat anti-rabbit (Life technologies, A11034, 1:300). Antibody specificity was confirmed using isotype control and by preincubating the anti-CD47 antibodies with recombinant CD47 antigen (R&D Systems) in a 1:5 ratio for 16h at 4 °C before application. High resolution imaging of the carotid sections was performed as previously described[34].

Murine cardiovascular tissue. *Atherosclerosis models.* In the atherosclerosis studies described below, a total of 179 male *apoE*-deficient mice on the C57BL/6 background (*apoE*$^{-/-}$, Jackson Laboratory, catalogue #002052) were used.

In the main atherosclerosis intervention studies, 8-week-old mice were implanted with subcutaneous Alzet minipumps (model 2004, Alzet Osmotic Pumps) containing Angiotensin II (AngII, Sigma-Aldrich, 1000 ng kg^{-1} min^{-1}) and initiated on a high fat Western diet (21% anhydrous milk fat, 19% casein and 0.15% cholesterol, Dyets no. 101511) for the ensuing 4 weeks, as previously described[19]. To determine the effect of CD47 signalling on vascular disease, mice were injected with either 200 μg of the inhibitory anti-CD47 antibodies (MIAP410, BioXcell, $n=18$) or IgG1 control (MOPC-21, BioXcell, $n=20$) IP QOD, at the dose previously studied[15]. The antibody therapy was started one day before the pump implantation. Animals were observed daily, and in the case of premature sudden death, necropsy was performed to determine the cause of mortality. Blood pressure in conscious mice was measured at baseline (after standard acclimatization with a Visitech Systems Inc. machine), and weekly for the duration of the study. At 12 weeks of age, the mice were killed after an overnight fast, with serum and visceral organs (including the aortae) isolated and processed for analysis.

In the chronic atherosclerosis studies, male *apoE*-deficient mice were weaned and initiated on a high fat diet at 4 weeks of age and maintained on this for the subsequent 12 weeks (without any angiotensin infusion). Antibody injection was performed as described above while the high fat diet was given ($n=9$ per condition), and the animals were killed at the age of 16 weeks.

In the established disease model, *apoE*-deficient mice were weaned onto a high fat diet at 4 weeks of age and continued on this for the ensuing 8 weeks (without any angiotensin infusion). At 12 weeks of age (after lesions had developed), mice were initiated on 200 μg of anti-CD47 antibodies ($n=14$) or IgG1 ($n=13$) IP QOD for the ensuing 6 weeks, and killed at 18 weeks of age.

In the TNF-α inhibitor synergy studies 8-week-old *apoE*-deficient mice were implanted with AngII pumps and maintained on Western high-fat diet, and then randomized to one of four groups, including the: (1) IgG group (mouse IgG and human Fc, $n=10$); (2) etanercept group (etanercept 0.2 mg per kg SQ weekly (Amgen) and mouse IgG IP QOD, $n=8$); (3) CD47 antibody group (MIAP410 50 μg IP QOD and human Fc SQ weekly, $n=16$); or (4) combination group (MIAP410 and etanercept, $n=19$)). In this model, the antibody treatment was started the day before AngII pump implantation and delivered for 4 weeks, and the mice were euthanized at 12 weeks of age. Note that in this model, the anti-CD47 antibody dose was reduced by 75% to determine whether a lower dose of therapy could also affect atherogenesis.

In the short-term intervention model, 8-week-old *apoE*-deficient mice were implanted with AngII pumps and maintained on Western high-fat diet without antibody therapy for the ensuing 23 days. Beginning at day 23, the mice received SQ injections of either: (1) IgG daily, $n=10$; (2) etanercept (0.8 mg per kg at day 23, $n=6$); (3) anti-CD47 antibody (200 μg of MIAP410 daily, $n=11$); or (4) combination therapy, $n=11$ between days 23 and 27. This cohort of mice was killed after only 5 days of antibody treatment (at day 28) and was used to evaluate the effect of antibody therapy in established atherosclerotic plaques of identical size.

To evaluate the effect of antibody therapy on atherosclerotic plaque vulnerability, we used the recently described 'tandem stenosis' model[35]. At 6 weeks of age, *apoE*-deficient mice were initiated on high-fat diet and maintained on this for ensuing 6 weeks. At 12 weeks of age, tandem stenoses were introduced in a manner shown to reproducibly alter shear stress and induce plaque rupture, as previously described[35]. Briefly, the mice were anaesthetized by isoflurane inhalation and an incision was made to allow dissection of the right common carotid artery from the circumferential connective tissues. Serial stenosis with a 150 μm outer diameter were then introduced 1 mm and 4 mm from the carotid bifurcation. The stenosis diameter was obtained by placing a 6–0 suture around the carotid artery together with a 150 μm needle that was tied to it and later removed. Antibody therapy was started the day before the surgery and continued thereafter. Mice were killed 7 weeks after the surgery and intraplaque haemorrhage was quantified within the processed tissue sections.

In addition to the mice treated with anti-CD47 antibody or control antibody, a separate cohort of 12 male *apoE*$^{-/-}$ mice were fed a high-fat diet for either 8, 12 or 20 weeks, but were not treated with antibody nor implanted with osmotic minipumps. These mice were used to determine aortic gene expression changes during atherogenesis, using the RNA analysis methods described below. In these experiments, comparison was made to control C57BL/6 mice fed standard chow diet for 24 weeks.

Finally, a cohort of 3 *apoE*$^{-/-}$ mice were implanted AngII osmotic pump and fed a high-fat diet for 4 weeks (but not treated with antibody) and then injected with biotin-labelled anti-CD47 antibodies 24 and 6 h before being killed, to determine where the therapeutic antibody accumulates *in vivo*. Nonatherosclerotic C57BL/6 and CD47-deficient mice (*Cd47*$^{-/-}$, Jackson Laboratory, catalogue #003173) were also injected with the biotin-labelled antibodies, and served as controls. All animals were analysed as described below.

Vascular tissue preparation, immunohistochemistry and atherosclerotic lesion quantification. Aortic atherosclerosis lesion area was determined as described previously[17]. Briefly, the arterial tree was perfused with PBS and then fixed with 4% PFA. The heart and the full-length of the aorta-to-iliac bifurcation was exposed and dissected carefully from any surrounding tissues. Thoracic aortas were then opened along the ventral midline and dissected free of the animal and pinned out flat, intimal side up, onto black wax. Aortic images were captured with a digital camera mounted on a Nikon stereomicroscope and analysed using Adobe Photoshop CS5 software. The percentage of lesion area was calculated as total lesion area divided by total surface area. The atherosclerotic lesions within the aortic valve area (aortic sinus) were analysed as described previously[17]. The samples were perfused with PBS, fixed with 4% PFA, embedded in OCT, and sectioned at 7-μM thickness. Four sections at 100-μM intervals were collected from each mouse and stained with ORO, Masson's trichrome, haematoxylin and eosin, smooth muscle α-actin (SMA, Abcam, ab5694, 1:300), Mac-3 (BD Sciences, BD 550292, 1:100), CD-3 (Abcam, ab5690, 1:150), and Ly-6G (BD Sciences, BD 551459, 1:300). Atherosclerosis burden was quantified from the luminal aspect of the blood vessel through the plaque to the internal elastic lamina (that is, lipid in the neointima was quantified). Necrotic core size was quantified by calculating the area of the lesion which was acellular on Masson's trichrome staining, as previously described[17,36]. Plaque haemorrhage was quantified by determining the presence or absence of red blood cells (TER-119, Santa Cruz Biotechnology) within the plaque, as previously described[37]. Subsequent immunohistochemical studies were quantified from the luminal aspect of the blood vessel through the plaque to the external elastic lamina (to assess changes which also involved the tunica media). To detect the localization of injected biotin-labelled anti-CD47 antibodies, the avidin–biotin complex technique was used. Frozen sections of aortic sinus were prepared from the mice injected with biotin-labelled anti-CD47 antibodies, as described above. Endogenous peroxide activity was blocked by incubation with 0.3% hydrogen peroxide for 30 min, and the sections were washed with water and PBS, followed by blocking with 5% goat serum for 30 min. Biotin was detected using Vecstatin ABC kit and DAB substrate kit per protocol (Vector laboratories). Corresponding aortic sinus sections from the mouse without biotin antibody injection were used as negative controls, as were *Cd47*$^{-/-}$ mice which had been injected as above. For immunoflourescent staining of these samples, sections were blocked with 5% goat serum for 30 min, then incubated with Streptavidin-Alexa Fluor 546 conjugate (Life Technologies, 1:300) and Mac-3 (BD, 1:100) for 1 h, followed by Alexa Fluor 488 donkey anti-rat (Life Technologies, 1:300). *In vivo* apoptosis was assessed by staining for TUNEL positivity with the Cell Death Detection Kit (Roche), per protocol, and confirmed with cleaved caspase 3 (Cell Signaling #9661, 1:200) staining followed by Alexa Fluor 488 goat anti-rabbit (Life technologies, 1:250). The cleaved-caspase-3-positive area was measured and quantified using Adobe Photoshop, and the percentage of positive area was calculated as total caspase-3-positive area divided by total atherosclerotic plaque area measured by ORO staining in the serial sections. To calculate the *in vivo* phagocytic index, we performed double staining of cleaved caspase 3 (detected with Alexa Fluor 488 goat anti-rabbit antibody) and Mac-3 (detected with Alexa Fluor 594 goat anti-rat antibody (Life technologies, 1:250)). The number of free apoptotic cells not associated with a macrophage (indicated by a star (Fig. 2f)) was manually assessed in a blinded fashion, and compared to apoptotic cells associated with a macrophage (indicated by an arrow), as previously described[2]. For phospho-SHP1 staining, the sections were stained with phospho-SHP1 antibodies (Abcam, ab131500, 1:50) and Mac-3 followed by Alexa Fluor. The phospho-SHP1-positive area was normalized to Mac-3-positive area. All lesion areas and indices were measured and quantified using Adobe Photoshop by a blinded observer. Samples collected from several tissue beds were also snap-frozen in liquid nitrogen for subsequent mRNA and protein expression analysis, as described below.

Vascular tissue electron microscopy. Electron microscopy was performed in the Stanford University Cell Sciences Imaging Facility, as previously described[17]. Briefly, samples were fixed and processed using standard histologic techniques then imaged using a JEOL JEM-1400 transmission electron microscope. Ingested apoptotic bodies (indicated by white arrow (Fig. 2g)), free apoptotic bodies (indicated by yellow arrow), and apoptotic bodies undergoing secondary necrosis (indicated by red arrow) were qualitatively assessed in a blinded manner, as previously described[17].

Serum and plasma analysis. Serum chemistry, lipid, complete blood count, and differential analyses were performed by the Stanford Animal Diagnostic Laboratory, as previously described[17]. In brief, blood samples were collected by cardiac puncture after an overnight fast. Automated haematology was performed on the Sysmex XT-2000iV analyser system. Blood smears were prepared for all full complete blood count samples and reviewed by a medical technologist. Chemistry analysis was performed on the Siemens Dimension Xpand analyser, and included analyses of renal function, electrolyte levels, liver function tests, fasting glucose levels and fasting lipid panels. A medical technologist performed all testing, including dilutions and repeat tests as indicated, and reviewed all data. Serum insulin levels were measured by ELISA kit according to the manufacturer's instruction (EMD Millipore).

Griess reaction. The activity of nitric oxide synthase was evaluated using a modified Griess assay. Lung samples were collected from mice and snap-frozen by liquid nitrogen before homogenization in PBS. The nitrate and nitrite levels were measured by Ultrasensitive Colorimetric Assay for nitric oxide synthase (Oxford Biomedical Research) according to the manufacture's instructions, and standardized by the protein amount.

Hybrid Mouse Diversity Panel. The Hybrid Mouse Diversity Panel (HMDP), which includes a quantitative analysis of 109 classical and recombinant inbred mouse strains[38], was used to identify factors associated with vascular CD47 expression, *in vivo*. Briefly, whole aorta from the arch to the mid-abdomen was snap-frozen at the time of death and total RNA was isolated using the RNeasy kit (Qiagen), as described[39]. Genome-wide expression profiles were determined by hybridization to Affymetrix HT-MG_430 p.m. microarrays on a subset of female mice from 104 strains ($n = 2$ aorta per strain). Quantification of plasma cytokines was carried out in a multiplexed immune-capture microbead system (Milliplex Mouse Cytokine/Chemokine Magnetic Bead Panel MCYTOMAG-70K, EMD Millipore) as per the manufacturer's instructions. Cytokines profiled were: G-CSF, GM-CSF, IFNr, IL-1α, IL-1β, IL-2, IL-4, IL-6, IL-7, IL-10, IL-12 (p40), IL-12 (p70), IL-13, IL-15, IP-10, KC, MCP-1, MIP-1α, MIP-1β, M-CSF, MIP-2, MIG, RANTES, TNF-α. Plasma insulin was measured using the mouse insulin ELISA kit (80-INSMS-E01, Alpco) as per the manufacturer's instructions. Pearson's correlations were generated to calculate transcript–transcript and transcript–trait correlations. Using these methods, the genes and plasma cytokines that were significantly associated with aortic CD47 expression levels were identified.

***In silico* bioinformatics methods.** *Pathway analysis.* Genome-wide correlation analyses were performed to identify genes that are significantly correlated with CD47 expression in the human and murine vascular tissue collections described above. These lists were intersected to identify genes that are commonly co-expressed across multiple data sets in both species. The resulting list of genes (Extended Data Fig. 7a) was subjected to a series of bioinformatics analyses including the Database for Annotation, Visualization and Integrated Discovery (DAVID), Kyoto Encyclopedia of Genomes and Genes (KEGG), Gene Ontology (GO), and Protein Analysis Through Evolutionary Relationships (PANTHER) classification. Additionally, genes were mapped to open chromatin regulatory intervals in primary human vascular cells and analysed using the Genomic Regions Enrichment of Annotations Tool (GREAT). Pathways found to be over-expressed were ranked by *P* value. Statistical overrepresentation and enrichment analyses were performed using Bonferroni correction for multiple testing ($P < 0.05$ cutoff).

Ingenuity Pathway Analysis (IPA) was then performed on the resulting intersected CD47 co-expression gene list from human carotid atherosclerosis (BiKE study) and murine aortic atherosclerosis (HMDP study). Briefly, the 63 gene identifiers and expression values were analysed using the Core pathway analysis after removing any duplicates and unmapped identifiers. The resulting networks were then subjected to an Upstream Regulators Analysis using the Ingenuity Knowledge Base after applying a filter to include all genes, RNAs and proteins, while excluding chemicals or drugs. Overlap *P* values were calculated for each upstream regulator using a Fisher's exact test and activation *z*-scores were calculated by comparing observed direction of target genes with inferred literature-derived regulatory direction to identify the most significant upstream regulators for CD47.

Promoter analysis. Using the UCSC browser, the genetic sequence 1 Kb upstream of the *CD47* promoter was identified and analysed, as previously described[17]. In addition to evaluating for open chromatin status and DNase hypersensitivity sites, potential transcription factor binding sites (TFBS) were predicted using the following online bioinformatics tools: TRANSFAC (BIOBASE), P-Match, TFSearch, Alibaba, PROMO, and MatInspector. High confidence binding sites (85% likelihood cutoff) were accepted for additional analysis. Additionally, the predicted binding sites in the *CD47* promoter region were intersected with open chromatin peaks identified from the assay for transpose accessible chromatin followed by sequencing (ATAC-seq) in primary human coronary artery SMCs (HCASMC).

Cell culture. Primary vascular SMCs were collected from the aortas of C57BL/6 mice and propagated in DMEM supplemented with 10% FBS, as previously described[17,40]. Human coronary artery SMCs (HCASMC, Lonza Catalog CC-2583, passage 3-6) were propagated in SmGM-2 growth media (Lonza) containing 5% FBS. To obtain human macrophages, leukocyte reduction system (LRS) chambers were obtained from the Stanford Blood Center from anonymous donors. Monocytes were purified on an autoMACS Pro Separator (Miltenyi) using whole-blood anti-CD14 microbeads (Miltenyi) and differentiated to macrophages by culture for 7-10 days in IMDM+GlutaMax (Invitrogen) supplemented with 10% AB-human serum (Gemini Bio-Products 100-512) and 100 U ml^{-1} penicillin and 100 μg ml^{-1} streptomycin (Invitrogen). RFP^{+} mouse macrophages were generated and evaluated as previously described[41]. Briefly, bone-marrow cells were isolated from C57BL/Ka Rosa26 mRFP1 transgenic mice and differentiated in IMDM + GlutaMax supplemented with 10% fetal bovine serum, 100 U ml^{-1} penicillin and 100 μg ml^{-1} streptomycin, and 10 ng ml^{-1} murine M-CSF (Peprotech). Mouse yolk sac endothelial cell line (C166, ATCC, CRL-2581) and mouse macrophage cell line (RAW 264.7, ATCC, TIB71) were grown in DMEM-growth media containing 10% FBS, while mouse T-lymphocyte cell line (EL4, ATCC, TIB-39) were grown in DMEM containing 10% horse serum. Human macrophage cell line (THP1, ATCC, TIB-202) were grown in RPMI-1640 medium containing 10% FBS and 0.05 mM 2-mercaptoethanol. Human embryonic kidney cells (HEK-293, ATCC, CRL-1573) used for luciferase reporter assays were grown in DMEM-growth media containing 10% FBS. No additional cell authentication or mycoplasma contamination testing was performed.

A variety of atherosclerosis-related or pro-apoptotic stimuli were applied to the cells in the experiments described below including: oxidized LDL (oxLDL, 50 μg ml^{-1}, Alfa Aesar), Ang II (100 nM, Sigma-Aldrich), fibroblast growth factor (FGF, 100 ng ml^{-1}, R&D), platelet-derived growth factor (PDGF, 100 ng ml^{-1}, R&D), and lipopolysaccharide (LPS, 1 μg ml^{-1}, Sigma-Aldrich). Additionally, a number of cytokines associated with CD47 expression through the HMDP Luminex array were also tested, including tumour necrosis factor α (TNF-α, 50 ng ml^{-1}, R&D), interleukin 2 (IL-2, 100 ng ml^{-1}, Biolegend), chemokine receptor ligand 1 (CXCL1, 100 ng ml^{-1}, Biolegend), interleukin 4 (IL-4, 50 ng ml^{-1}, Biolegend), and transforming growth factor β (TGF-β, 50 ng ml^{-1}, R&D). Before experimentation, SMCs were serum-starved for 24 h in DMEM and then stimulated with the stimuli listed above for 24 h before analysis. In some experiments, the cells were stimulated with staurosporine (STS, 1 μM, Sigma-Aldrich) for 1 or 4 h to induce apoptosis, after 24 h of TNF-α treatment.

To inhibit TNF-α signalling, a chemical inhibitor (SPD 304, Sigma Aldrich) or a monoclonal antibodies (Infliximab, Janssen) were used. Briefly, TNF-α was pre-incubated with 10 μM of SPD304 or 100 μg ml^{-1} of infliximab in serum free DMEM for 20 min before cell stimulation. To inhibit NF-κB signalling, the cells were pre-treated with 10 μM BAY 11-7085 (Santa Cruz Biotechnologies) or DMSO, then stimulated with TNF-α.

For MAPK western blotting experiments, mouse aortic SMCs were serum-starved for 48 h, pre-treated with 10 μg ml^{-1} of CD47 antibodies or IgG for 20 min, then stimulated with thrombospondin-1 (TSP1, 10 μg ml^{-1}, R&D) for 10 or 30 min. For eNOS western blotting experiments, C166 cells were serum-starved for 8 h, pre-treated with 2 μM TSP1 with or without 10 μg ml^{-1} of CD47 antibody or IgG for 20 min, then stimulated with acetylcholine (Ach, 10 μM, Sigma-Aldrich) for 15 min.

mRNA isolation and quantitative reverse-transcription PCR. RNA was isolated from cell lysates using the miRNeasy Mini Kit (Qiagen) according to the manufacturer's protocol. RNA was isolated from murine organ samples using the Trizol method (Invitrogen). RNA was quantified with the Nanodrop machine (Agilent Technologies). For quantitation of gene transcription, cDNA was generated with MultiScribe reverse transcriptase (Applied Biosystems), and then amplified on the ABI PRISM 7900HT with commercially available TaqMan primers (Applied Biosystems) and normalized to 18S internal controls, as previously described[17]. A list of the primers and probes used in these studies is provided in Extended Data Table 1e.

Protein extraction and western blotting. Total protein was isolated from cultured cell lines and tissue homogenates using 1× cell lysis buffer (Cell Signaling) supplemented with 1× Halt Protease & Phosphatase Single-Use Inhibitor Cocktail (Thermo Scientific), as previously described[17]. The protein concentration in each sample was measured using Pierce BCA Protein Assay Kit (Thermo Scientific). Equal amounts of protein were loaded and separated on precast gels (Bio-Rad) and thereafter transferred onto PVDF membranes (Bio-Rad). Following a 1 h incubation in 5% bovine albumin serum solution prepared in 1× TBST, these membranes were probed with commercially available antibodies designed to recognize endogenous P38 (Cell Signaling, 1:1000), phospho-P38 (Cell Signaling, 1:1000), ERK1/2 (Cell Signaling, 1:1000), phospho-ERK1/2 (Cell Signaling, 1:1000), phospho-eNOS (Cell Signaling, 1:1000), CD47 (Novus Biologicals, 1:1000) and *GAPD* (1:1000; Cell Signaling Technologies) overnight at 4 °C. Membranes were rinsed with TBST and incubated with appropriately matched horse-radish peroxidase (HRP)-conjugated anti-mouse (1:5000; Life Technologies) or anti-rabbit (1:5000; Life Technologies) antibodies for 1 h, before protein expression was detected using SuperSignal West Pico Chemiluminescent substrate (Thermo Scientific). Membranes were then scanned with a Licor Odyssey Fc imager for quantitative analysis. In some experiments, membranes loaded with protein were incubated with anti-CD47 antibody that had been preabsorbed with CD47 peptide (R&D systems, 1866-CD, 1:5 dilution) for 16 h, to determine the specificity of the primary antibody.

Apoptosis assays. To evaluate apoptosis, the luminometric Caspase-Glo 3/7 Assay (Promega, G8090) was performed on cultured cells, according to the manufacturer's protocol. Briefly, mouse aortic SMCs were seeded in 96-well plates at the density of 10,000 cells per well, grown at 37 °C for 24 h, and then serum-starved for 24 h. Apoptosis was induced with 1 μM STS treatment for 4 h in the presence of 10 μg ml^{-1} of anti-CD47 antibodies or IgG. Confirmatory assays were performed by flow cytometry, where cells where exposed to 24 or 72 h of vehicle, 50 ng ml^{-1} of TNF-α, or 50 μg ml^{-1} of oxLDL, then treated with 1 μM STS for 4 h before being collected in TrypLE. These cells were stained with anti-annexin V antibody labelled with fluorescein isothiocyanate (FITC) and propidium iodide (eBioscience) and analysed by Scanford cell analyser (Stanford Shared facility, Stanford), as previously described[42]. These FACS data was analysed by FlowJo 10.1r5.

Proliferation assays. A modified MTT (3-[4,5-dimethyl-thiazol-2-yl]-2,5-diphenyltetrazolium bromide) assay was performed to analyse SMC proliferation and viability. Mouse aortic SMCs were seeded in 96-well plates at the density of 6,000 cells per well, grown at 37 °C overnight, and then serum-starved for 48 h. The cells were stimulated with 10% serum or 10 μg ml^{-1} TSP1 with or without 10 μg ml^{-1} of anti-CD47 antibodies or IgG for 24 h and then incubated for 4 h in the presence of 10 μl of MTT AB solution (Millipore). The formazan product was dissolved by addition of 100 μl acidic isopropanol (0.04 N HCl) and absorbance was measured at 570 nm (reference wavelength 630 nm) on an ELISA plate reader by SpectraMax 190 Microplate Reader (Molecular Devices).

Efferocytosis assay. Standard *in vitro* phagocytosis assays were performed as previously described[41]. SMCs were labelled with 2.5 μM carboxyfluorescein succinimidyl ester (CFSE) according to the manufacturer's protocol (Invitrogen). 100,000 SMCs were plated per well in a 96-well plate (Corning) and pre-incubated with antibody (IgG1 isotype control (MOPC-21) or MIAP410 (anti-CD47)) for 30 min at 37 °C. An unrelated anti-CD8 antibody was also tested as a negative control. After 30 min, 50,000 macrophages were added to each well and co-incubated for 2 h in serum-free medium, then analysed using an LSRFortessa cell analyser with high throughput sampler (BD Biosciences). RFP^{+} mouse macrophages were identified by intrinsic fluorescence. Dead cells were excluded from the analysis by staining with DAPI (Sigma). Phagocytosis was evaluated as the percentage of GFP^{+} macrophages using FlowJo X 10.0.7r2 (Tree Star) and was normalized to the maximal response by each independent donor against each cell line. In addition to measuring basal efferocytosis rates, experiments were repeated with target cells that had been pretreated with a variety of compounds (alone or in combination) including STS, oxLDL, TNF-α, TSP1, and infliximab. Confirmatory assays were

performed with RAW macrophages where target cells were labelled with 1 μM of CellTracker Deep Red dye (Life technologies) and phagocytes were labelled with 1.25 μM of CellTracker Orange CMRA (Life technologies) at 37 °C for 30 min. As above, cells in these assays were treated with 50 μg ml^{-1} of oxLDL, 50 ng ml^{-1} of TNF-α, or 100 μg ml^{-1} of infliximab antibody for 24 h before co-culture in serum-free medium with 10 μg ml^{-1} of antibody of IgG1 isotype control (MOPC-21) or anti-CD47 (MIAP410) for 2 h at 37 °C. Double-positive cells were quantified using the Scanford cell analyser (Stanford Shared facility) and analysed by FlowJo 10.1r5, as previously described[17]. Statistical significance was determined by one-way or two-way ANOVA with Bonferroni's correction using Prism 5 (Graphpad).

Flow cytometry. To measure the cell surface expression of CD47, cells were exposed to vehicle or 50 ng ml^{-1} of TNF-α for 24 h. In some experiments, cells were treated with 1 μM STS during the last 1 h or 4 h of the incubation, before analysis. The cells were collected in TrypLE (Life Sciences) and stained with anti-CD47 antibodies (AbD Serotec MCA2514GA, clone1/1A4, 1:400) or IgG (eBioscience), followed by Alexa Fluor 488 goat anti-mouse (Life Technologies, 1:400), and then FACS-sorted within 1 h (BD FACSCaliber, 530 nm fluorescence [FL1] and >575 nm [FL3]). Analysis was performed with FloJo 7.6.3.

Immunocytochemistry. Primary mouse aortic SMCs were seeded at approximately 60% confluence in glass-bottom culture dishes (MatTek Corporation). Following treatment with TNF-α and/or STS, as described above, cells were rinsed with PBS and fixed with freshly prepared 4% PFA (Fisher Scientific). Once permeabilized with 0.1% Triton X-100 (Sigma), cells were incubated with blocking buffer (3% BSA, Cell Signaling Technology) for 1 h and then incubated overnight at 4 °C with a CD47 antibody (1:80; R&D Systems, Cat# AF1866-SP). After rinsing with PBS, cells were incubated in the dark with a donkey anti-goat Alexa Fluor 594 conjugate secondary antibody (1:1000; Life Technologies) for 1 h then briefly incubated with DAPI. CD47 and DAPI localization was captured at 20× magnification using a Leica DMI3000 B microscope capable of taking fluorescent images. Studies using primary human coronary artery SMCs were also performed as above, but used 5% goat serum blocking buffer (ThermoFisher Scientific), and the following primary and secondary antibodies: CD47 antibody (Novus Biologicals, 1:50); HMGB1 (abcam, ab18256 1:100)); Alexa Fluor 594 goat anti-mouse (Life Technologies A11005, 1:300); and Alexa Fluor 488 goat anti-rabbit (Life Technologies, A11034). In some studies, exogenous CD47 peptide was preincubated with the cells before the CD47 antibody was applied, as described above.

Luciferase reporter assay. CD47 LightSwitch Promoter Reporter GoClones (RenSP, S710450), empty promoter vectors (S790005) and Cypridina TK Control constructs (pTK-Cluc, SN0322S) were obtained from SwitchGear Genomics and transfected into HEK cells using lipofectamine 2000 (Invitrogen). For overexpression assays, expression plasmids for *Nfkb1 (p50)*, *Rela (p65)*, *Nfkb2 (p52)*, and *c-Rel* were obtained from Addgene (#21965, #21966, #23289, #27256, respectively). Empty vector pCMV4 was generated by HindIII digestion of #21966, and pcDNA3.1 was obtained from Life Technologies. 50 ng of plasmid was co-transfected with 45 ng of the RenSP reporter and 5 ng of the pTK-Cluc reporter construct. Media was changed to fresh DMEM and 50 ng ml^{-1} of TNF-α was added 2, 8, 24, and 36 h before collection. The cell lysate and supernatant were collected 48 h after transfection and dual luciferase activity was measured with the LightSwitch Dual Assay System using a SpectraMax L luminometer (Molecular Devices), according to the manufacturer's instructions. Relative luciferase activity (*Renilla*/*Cypridina* luciferase ratio) was quantified as the percentage change relative to the basal values obtained from control-transfected cells not exposed to TNF-α treatment.

Chromatin immunoprecipitation. Chromatin immunoprecipitation (ChIP) was performed according to the Millipore Magna-ChIP protocol with slight modifications. HCASMC were cultured in normal growth media until approximately 75% confluent. Cells were fixed in 1% formaldehyde for 10 min to cross-link chromatin, followed by quenching with glycine for 5 min at room temperature. 2×10^7 cells per condition were collected, and nuclear lysates were prepared according to the manufacturer's protocol. Cross-linked chromatin nuclear extracts were sheared into approximately 500 bp fragments using a Bioruptor (Diagenode) for 3 cycles of 3 min (30 s on, 30 s off). Sheared chromatin was clarified via centrifugation at 4 °C for 10 min. 1×10^6 nuclei per condition was incubated with 2 μg rabbit IgG or anti-NF-κB p105/p50 antibody (Abcam, Ab7971) plus protein A/G magnetic beads overnight at 4 °C on a rotating platform to capture the protein–DNA complexes. Complexes were washed in low salt, high salt, LiCl, and TE buffers and then eluted with a ChIP Elution Buffer containing Proteinase K. Free DNA was subsequently purified using spin columns. Total enrichment was measured using primers designed based on the sequence of the top *NfkB* binding site within the *CD47* promoter: forward (−804 to −781): 5′-ATAGGGAAGAGCAGAGCGAGTAGA-3′ and reverse (+627 to +609): 5′-GCGTGGACCAGGACACCTA-3′), or a negative control region using the following primers: forward: 5′-CCGGAAGCACTTCTCCTAGA-3′ and reverse: 5′-AAGAGAGAGCGGAAGTGACG-3′. Quantitative real-time PCR (ViiA 7, Life Technologies) was performed using SYBR Green (Applied Biosystems) assays and fold enrichment was calculated by measuring the $\Delta\Delta C_t - \Delta\Delta C_t$ IgG. Melting curve analysis was also performed for each ChIP primer. Data are presented as the percentage of input DNA and as fold enrichment of chromatin precipitated with the NF-κB antibodies relative to the control IgG. In some experiments, cells were treated with TNF-α for 90 min and 24 h before isolation of nuclear lysates.

Statistical analysis. Aside from the microarray data (described above), all experimental data are presented as mean ± s.e.m. Data were subjected to the Kolmogorov–Smirnov test to determine distribution. Groups were compared using the Mann–Whitney *U* test for non-parametric data or the two-tailed Students *t*-test for parametric data. When comparing multiple groups, data were analysed by analysis of variance with one way ANOVA followed by Tukey's or Dunnett's post-hoc test. For multiple testing of parametric data, a value of $P < 0.05$ was considered statistically significant. *In vitro* experiments were replicated at least in triplicate and all analyses were performed in a blinded fashion by two separate investigators, unless otherwise specified. In the *in vivo* intervention studies, comparison was made between mice treated with anti-CD47 antibodies and IgG. In the *in vivo* synergy studies, ANOVA was performed as above with multiple comparison and linear trend post-testing across all four groups. In the *in vitro* studies, comparison was made between the intervention (anti-CD47 antibodies) and control (IgG) arms. 'Vehicle control' was only used in experiments where an additional treatment (for example, TNF, oxLDL, infliximab) was studied. In the TaqMan-based CD47 expression experiments, changes were demonstrated as mRNA fold-change compared to the baseline condition (set as '1'). In the microarray-based experiments, relative expression differences were displayed across conditions (for example, atherosclerosis versus no atherosclerosis). In the *in vitro* phagocytosis assays, efferocytosis rates are displayed as percent of maximum, as previously described[41]. Statistical analysis was performed with GraphPad Prism 5. Aside from the human plaque microarray studies (displayed as Tukey box plots) and the correlation plots (displayed as the 95% confidence band of the best fit line), all error bars display the standard error of the mean.

Study approval. All animal studies were approved by the Stanford University Administrative Panel on Laboratory Animal Care (protocol 27279) and conform to the Guide for the Care and Use of Laboratory Animals published by the US National Institutes of Health (NIH Publication No. 85-23, revised 1996). All human studies were performed with written informed consent and with the approval of the Ethical Committee of Northern Stockholm (BiKE).

31. Saksi, J. *et al.* Gene expression differences between stroke-associated and asymptomatic carotid plaques. *J. Mol. Med. (Berl.)* **89,** 1015–1026 (2011).
32. King, J. Y. *et al.* Pathway analysis of coronary atherosclerosis. *Physiol. Genomics* **23,** 103–118 (2005).
33. Ashley, E. A. *et al.* Network analysis of human in-stent restenosis. *Circulation* **114,** 2644–2654 (2006).
34. Perisic, L. *et al.* Gene expression signatures, pathways and networks in carotid atherosclerosis. *J. Intern. Med.* **279,** 293–308 (2016).
35. Chen, Y. C. *et al.* A novel mouse model of atherosclerotic plaque instability for drug testing and mechanistic/therapeutic discoveries using gene and microRNA expression profiling. *Circ. Res.* **113,** 252–265 (2013).
36. Jun, J. *et al.* Effect of intermittent hypoxia on atherosclerosis in apolipoprotein E-deficient mice. *Atherosclerosis* **209,** 381–386 (2010).
37. Alexander, M. R. *et al.* Genetic inactivation of IL-1 signaling enhances atherosclerotic plaque instability and reduces outward vessel remodeling in advanced atherosclerosis in mice. *J. Clin. Invest.* **122,** 70–79 (2012).
38. Yang, H. *et al.* A customized and versatile high-density genotyping array for the mouse. *Nat. Methods* **6,** 663–666 (2009).
39. Ghazalpour, A. *et al.* Comparative analysis of proteome and transcriptome variation in mouse. *PLoS Genet.* **7,** e1001393 (2011).
40. Rong, J. X., Shapiro, M., Trogan, E. & Fisher, E. A. Transdifferentiation of mouse aortic smooth muscle cells to a macrophage-like state after cholesterol loading. *Proc. Natl Acad. Sci. USA* **100,** 13531–13536 (2003).
41. Weiskopf, K. *et al.* Engineered SIRPα variants as immunotherapeutic adjuvants to anticancer antibodies. *Science* **341,** 88–91 (2013).
42. Leeper, N. J. *et al.* Loss of CDKN2B promotes p53-dependent smooth muscle cell apoptosis and aneurysm formation. *Arterioscler. Thromb. Vasc. Biol.* **33,** e1–e10 (2013).

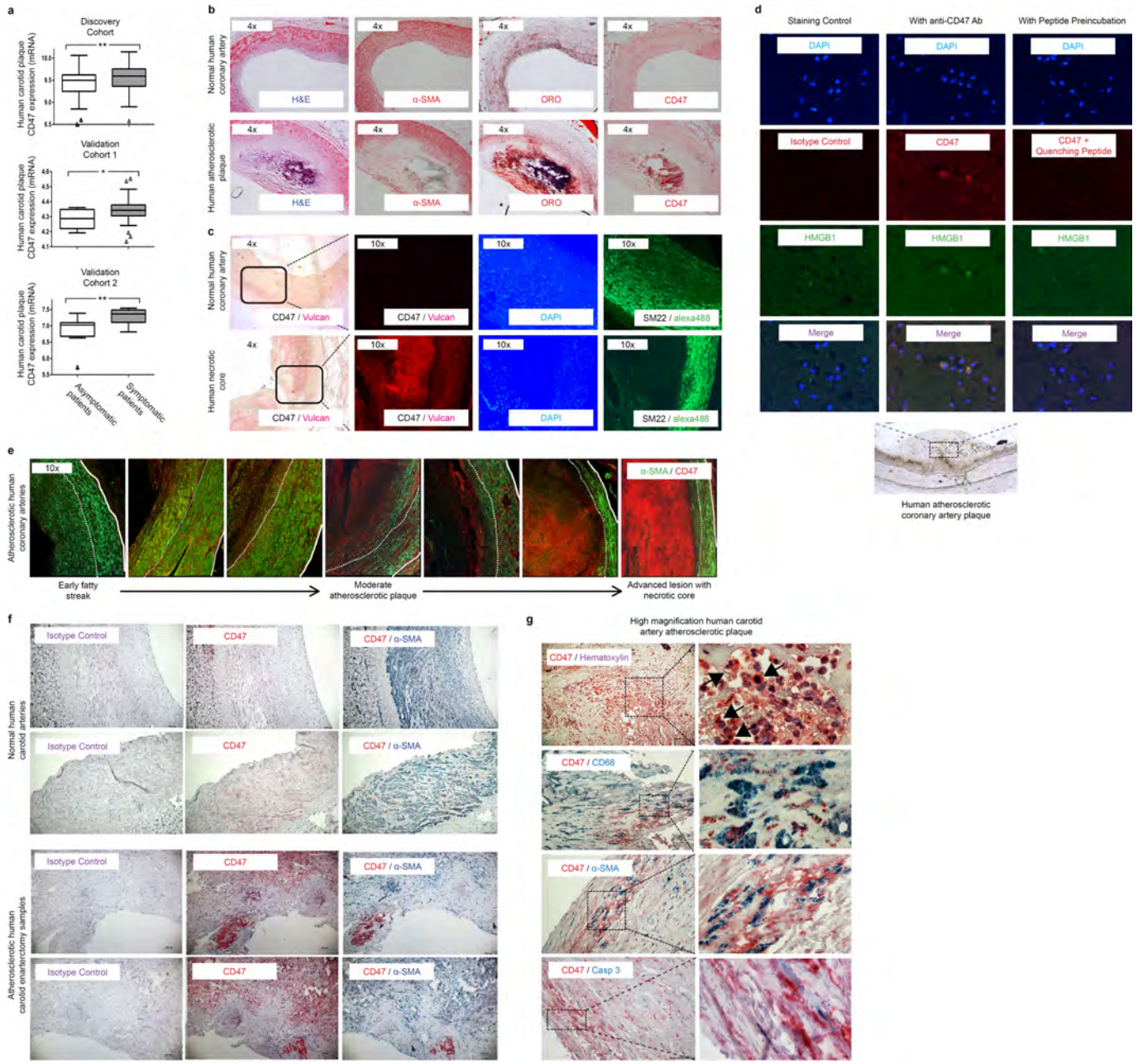

Extended Data Figure 1 | CD47 expression correlates with risk for clinical cardiovascular events and is progressively upregulated in the necrotic core of human blood vessels during atherogenesis. a, cDNA microarray expression profiling in the BiKE carotid endarterectomy biobank reveals that the relative expression of CD47 is increased in vascular homogenates taken from subjects with symptomatic disease (stroke or transient ischaemic attack, $n = 85$) compared to those with stable, asymptomatic lesions ($n = 40$). Similar findings were observed in the non-overlapping discovery and validation cohorts from BiKE ($n = 55$), and a second validation cohort from the Helsinki Carotid Endarterectomy Study (HeCES, $n = 21$). Data presented as Tukey box plots. **b**, Immunohistochemical staining reveals that CD47 co-localizes with lipidated plaque within human coronary lesions, as measured by Oil-Red-O (ORO) staining. **c**, Immunofluorescence staining of coronary samples confirms that CD47 is upregulated within the necrotic core. **d**, High magnification (40×) imaging of atherosclerotic coronary plaque confirms that CD47 expression is present on the surface of nucleated cells undergoing cell death, as indicated by HMGB1 staining. Specificity of the anti-CD47 antibody is confirmed in assays where the signal was quenched by preincubating the sections with recombinant CD47 peptide before primary antibody exposure. **e**, Additional representative coronary artery segments spanning the spectrum of progressive coronary artery disease (non-atherosclerotic coronary, early 'fatty streak', inwardly remodelled plaque, and advanced ulcerated lesion with necrotic core) confirm that CD47 is progressively upregulated during the development of coronary artery disease. The tunica media is indicated by dotted lines. **f**, Additional staining in human carotid artery sections confirms that CD47 expression is upregulated in atherosclerosis relative to healthy tissue, and appears most pronounced within the necrotic core. **g**, High magnification (100×) imaging confirms that the CD47 expression is specific to lesional cells, including SMCs (α-SMA), macrophages (CD68) and cells undergoing programmed cell death (Casp3). Comparisons made by two-tailed *t*-tests. $^{**}P < 0.01$, $^{*}P < 0.05$. Original magnification, ×40 (**d**), ×4 (**f**, **g**).

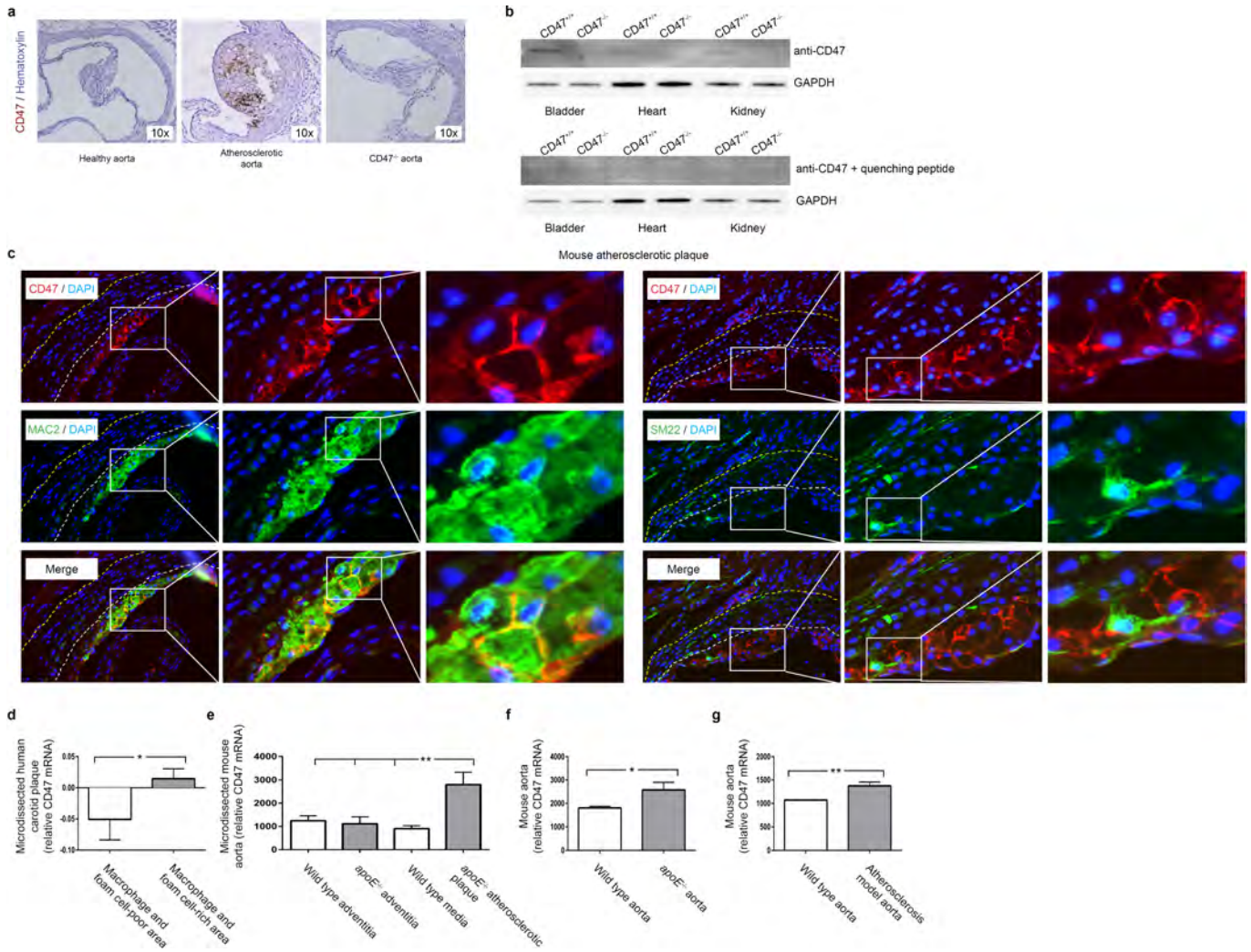

Extended Data Figure 2 | CD47 expression is increased in mouse models of atherosclerosis. a, Mice injected with biotin-labelled anti-CD47 antibodies reveal that these antibodies accumulate in the vasculature of atherosclerotic mice (middle), relative to non-atherosclerotic control mice (left). No staining is detected in $Cd47^{-/-}$ mice (right), indicating specificity of the antibody. **b**, Western blotting of tissue homogenates obtained from wild-type and $Cd47^{-/-}$ mice (with and without quenching CD47 peptide) further confirms the specificity of the antibody. For gel source data, see Supplementary Fig. 1. **c**, High resolution immunofluorescence staining of murine atherosclerotic plaques indicate that CD47 is specifically expressed on the surface of lesional cells, rather than extracellular debris. Original magnification, ×40. **d**, Publically available microarray data from laser capture microdissected (LCM) vascular tissue reveals that CD47 expression is increased within the macrophage and foam-cell-rich area of human plaque, relative to macrophage and foam-cell-poor areas (GSE23303). **e**, Similar results were observed in LCM tissue from mouse atherosclerotic plaque tissue, relative to non-atherosclerotic medial and adventitial tissue (GSE21419). **f**, **g**, Additional results from the Gene Expression Omnibus (GEO) database reveal that aortic CD47 expression is upregulated in murine models of atherosclerosis, as observed in the current study (GSE2372 and GSE19286). $^{**}P < 0.03$, $^{*}P < 0.05$.

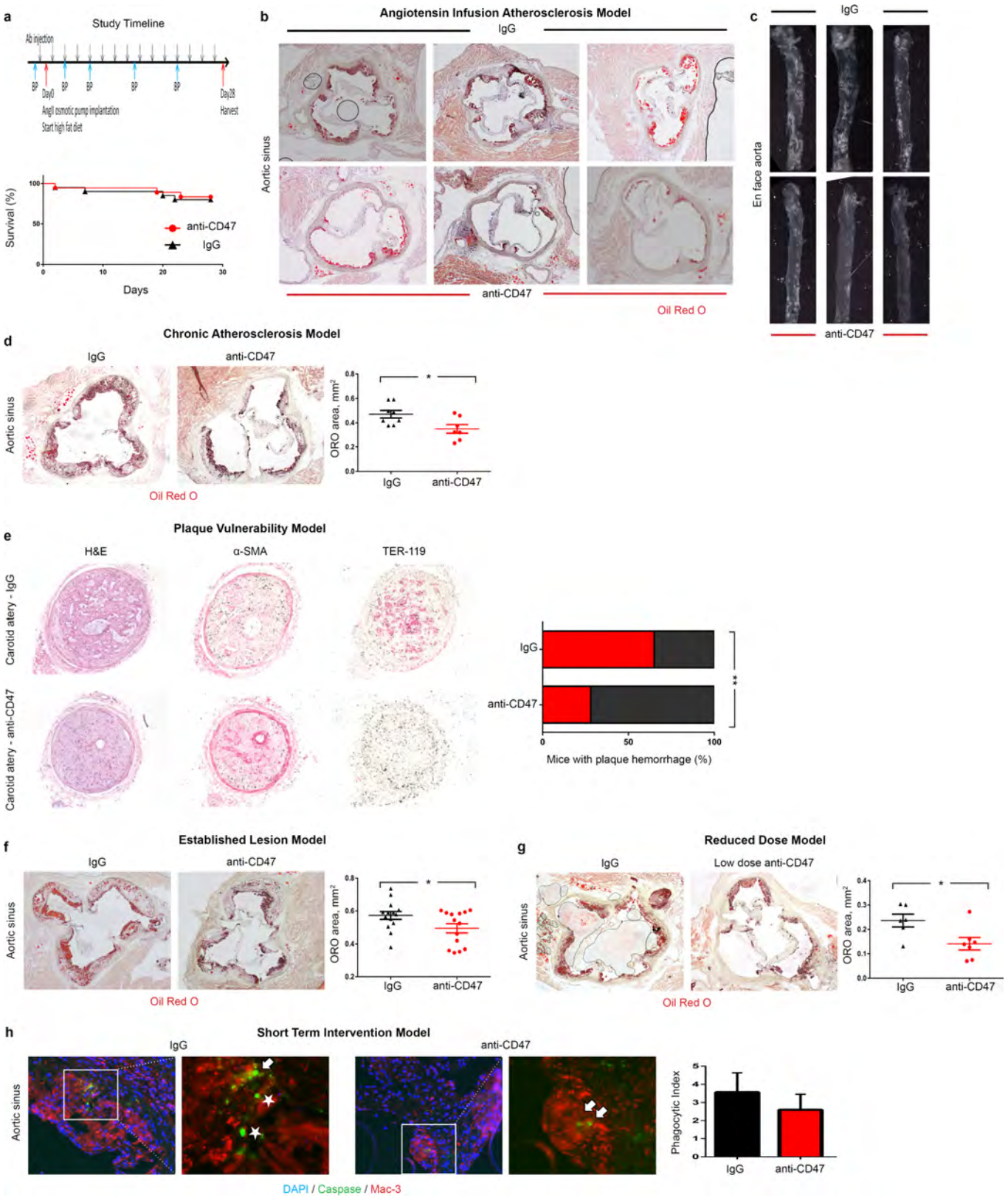

Extended Data Figure 3 | See next page for caption.

Extended Data Figure 3 | Anti-CD47 antibody reduces atherosclerotic burden in several orthogonal *in vivo* models. a, Study timeline detailing osmotic minipump implantation and high-fat feeding to induce atherosclerosis in the *apoE*$^{-/-}$ and 'angiotensin infusion' model used herein. Kaplan–Meier curves indicate no change in mortality with anti-CD47 treatment during 28 days of follow up. **b**, **c**, Additional representative examples confirm that anti-CD47 antibody reduces atherosclerosis content in the aortic sinus (**b**) and reduces the percentage of the *en face* aorta covered by atherosclerotic plaque (**c**). **d**–**g**, Several additional atherosclerosis models were also used in this study to confirm the beneficial effects of anti-CD47 antibody therapy, and to model additional aspects of human cardiovascular disease, including a 'chronic atherosclerosis' model, where antibody therapy was given for 12 weeks (with no angiotensin infusion) (**d**); a 'plaque vulnerability' model, where the impact of antibody therapy on plaque rupture and intraplaque haemorrhage was quantified (**e**); an 'established disease' model, where therapy was given for 7 weeks after mice had already developed advanced plaques of equivalent size (**f**); and a 'reduced dose' model, where the dose of anti-CD47 antibody was reduced by 75%, relative to the preceding studies (**g**). **h**, Additionally, a 'short term' study was performed where mice with established lesions of equivalent size and identical apoptosis rates were pulsed for only 5 days with anti-CD47 antibodies before collection, to quantify the effect of therapy on efferocytosis rates, independent of lesion size (phagocytic index indicated by the ratio of 'free' (white stars) to 'associated' (white arrows) apoptotic bodies). Additional methodological details are provided in the Methods. Comparisons made by two-tailed *t*-tests. $^{**}P < 0.03$, $^{*}P < 0.05$. Error bars represent the s.e.m. Original magnification, ×4 (**b**, **d**–**f**), ×2 (**c**), ×10 (**h**).

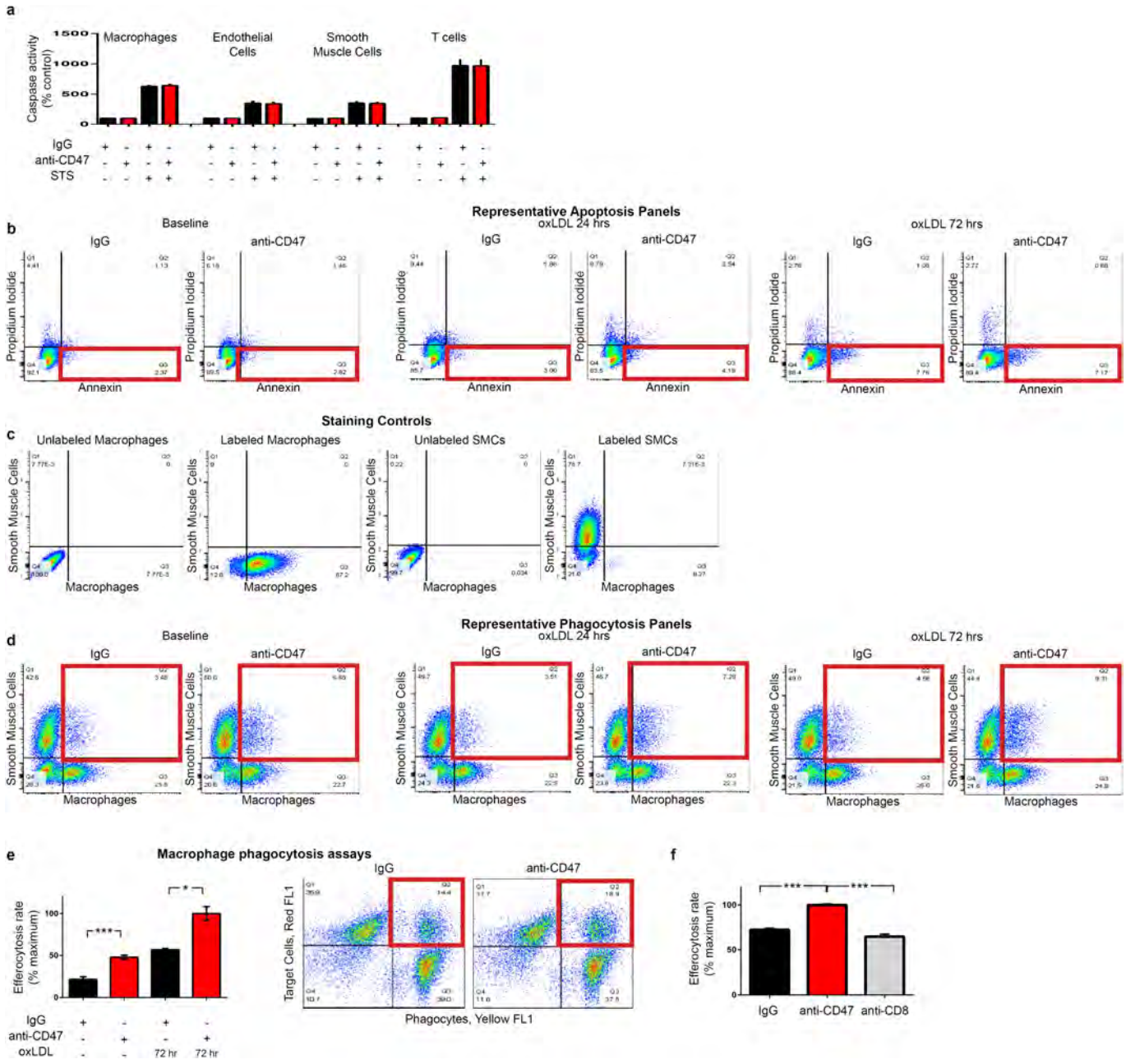

Extended Data Figure 4 | Anti-CD47 antibody promotes the phagocytosis of diseased SMCs and macrophages, without altering apoptosis. a, *In vitro* caspase activity assays reveal that anti-CD47 antibody does not alter rates of programmed cell death in any vascular cell type. **b**, Flow cytometry assays confirm that anti-CD47 antibody has no effect on apoptosis at baseline, or in vascular SMCs exposed to 24 or 72 h of oxLDL. **c**, Staining controls for the *in vitro* phagocytosis assays. **d**, Representative FACS plots for the *in vitro* efferocytosis conditions displayed in Fig. 2e. The right upper quadrant (highlighted in red) includes double-positive cells that are taken to represent a macrophage that has ingested a target cell. **e**, *In vitro* efferocytosis assays using lipid-loaded macrophages as the target cell confirm that anti-CD47 antibody also stimulates the clearance of this vascular cell type, similar to the findings observed with SMCs. **f**, Additional *in vitro* efferocytosis assays confirm that anti-CD47 antibody stimulates phagocytosis of vascular cells in a specific manner. Error bars represent the s.e.m.

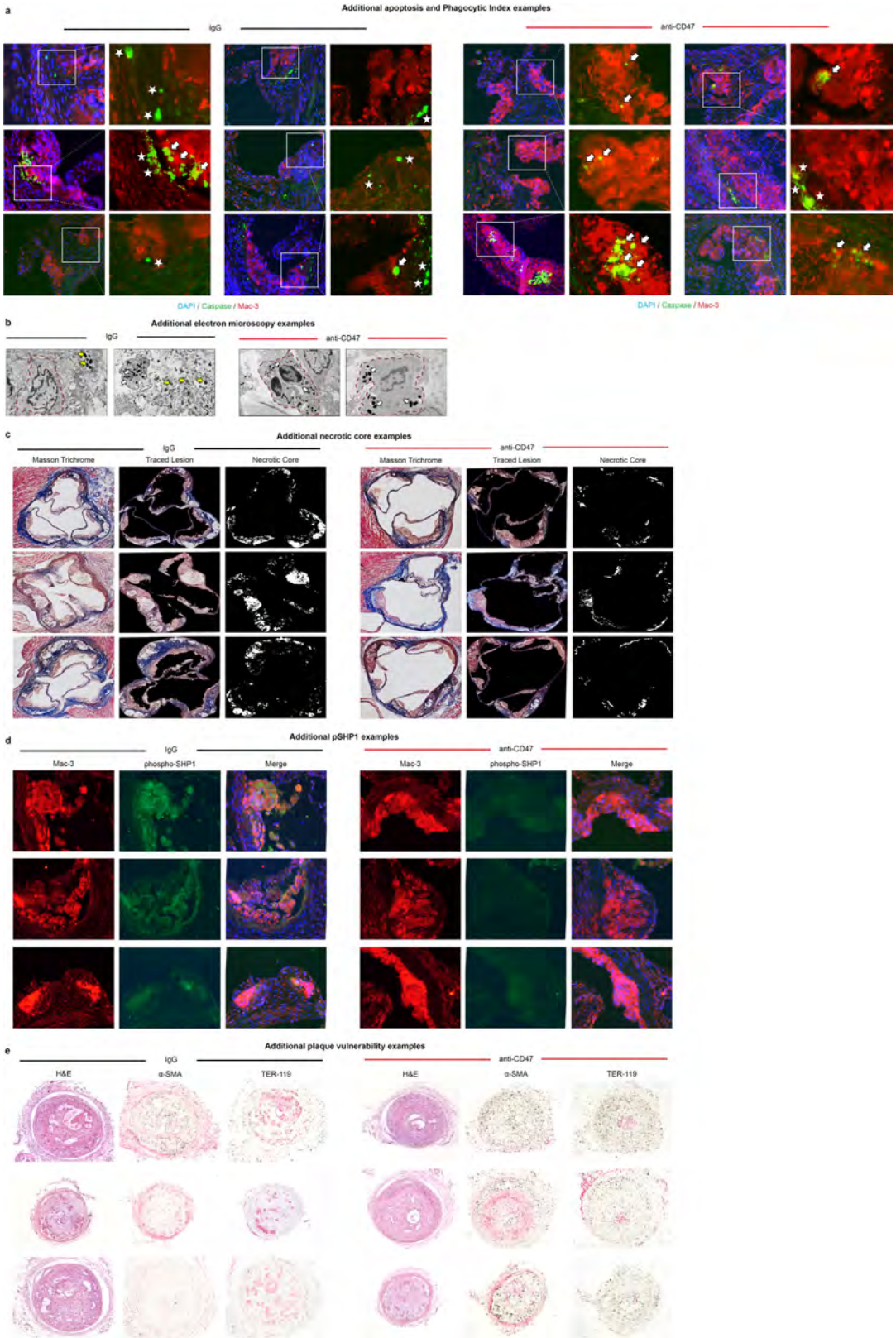

Extended Data Figure 5 | Additional examples confirm the pro-efferocytic properties of anti-CD47 antibody *in vivo*. **a**, Additional representative images detail that mice treated with anti-CD47 antibodies have a lower overall burden of apoptotic debris (caspase in green), as well as fewer examples of 'free' apoptotic bodies (white stars). Those apoptotic bodies that are present in these lesions are more often found in close proximity to macrophages (Mac-3 in red) and are considered 'associated' with a phagocyte if physically co-localized (white arrows). **b**, Additional electron microscopy examples provide further qualitative evidence that phagocytes present in the lesions of mice treated with anti-CD47 antibodies are more likely to have ingested several apoptotic bodies (white arrows) compared to lesions from IgG treated mice which are more likely to have a high burden of 'free' apoptotic bodies (yellow arrows). **c**–**e**, Additional representative examples of the necrotic core analysis (**c**), the phospho-SHP1 staining (**d**), and the plaque haemorrhage analysis (**e**) are shown, as described in the Methods. Original magnification, ×10 (**a**, **d**), ×4 (**c**, **e**).

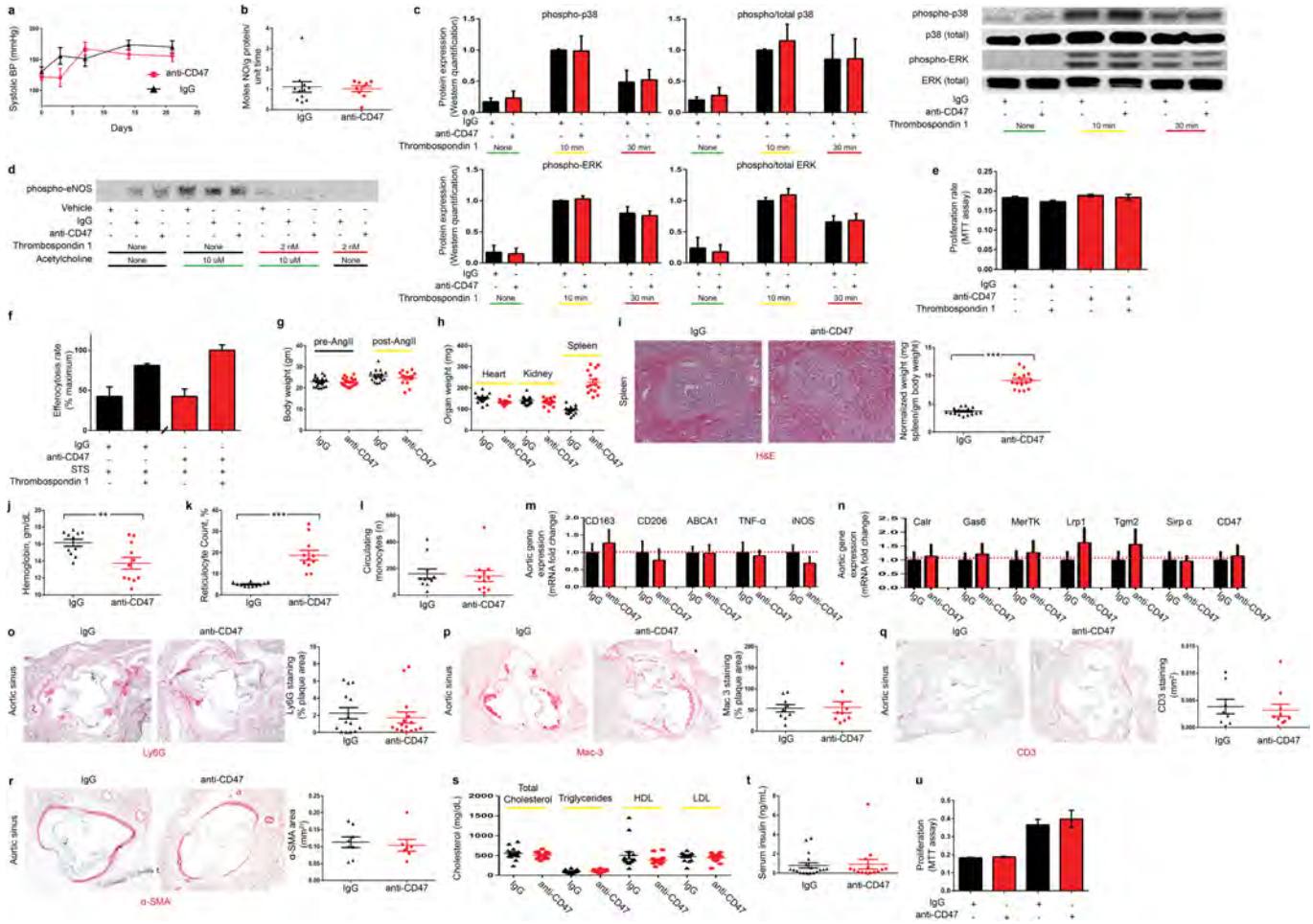

Extended Data Figure 6 | Full-dose anti-CD47 antibody therapy induces anaemia, but does not appear to alter NO elaboration, TSP1-dependent signalling, or other processes relevant to vascular biology. **a**, No significant change in blood pressure is observed between mice treated with IgG or anti-CD47 antibodies, arguing against a systemic difference in nitric oxide (NO) production due to antibody therapy. **b**, Direct measurement of pulmonary NO release via the Griess reaction indicates that anti-CD47 antibody does not increase NO elaboration *in vivo*. **c**, Western blot analysis of cultured murine vascular cells reveals that anti-CD47 antibody has no effect on the expected induction of p38 and ERK phosphorylation secondary to TSP1 treatment. **d**, Similarly, anti-CD47 antibody has no effect on TSP1-dependent inhibition of eNOS phosphorylation, nor acetylcholine-dependent induction of eNOS phosphorylation. **e**, MTT assays show that anti-CD47 antibody does not affect cellular proliferation rates in the presence of TSP1. **f**, *In vitro* efferocytosis assays show that the expected basal increase in phagocytosis observed after apoptotic cells are exposed to TSP1 (black bars) is not altered in the presence of anti-CD47 antibodies (red bars). (**g**). Compared to mice receiving control IgG, mice receiving anti-CD47 antibody treatment have similar body weights at baseline and at time of killing. **h**, No difference is observed for the weight of any organ between groups, with the exception of splenomegaly observed in the anti-CD47-treated animals. **i**, Histological analysis of the explanted splenic tissue reveals an increase in the red pulp of anti-CD47 treated mice without any change in fibrosis or white pulp content, suggestive of increased erythrophagocytosis in this reticuloendothelial organ. **j**–**l**, Dot plots detail the haemoglobin count (**j**), reticulocyte count (**k**) and circulating monocyte count (**l**) for each animal in the acute 4-week angiotensin-infusion atherosclerosis model. Note that this anaemia appears to be self-limited, and no anaemia was observed in the chronic atherosclerosis model or the reduced dose model ($P = 0.54$ and 0.57, respectively). **m**, mRNA analysis of aortic tissue reveals that anti-CD47 antibody has no significant effect on the expression of macrophage-polarization factors *in vivo*. **n**, Anti-CD47 antibody also has no effect on the aortic expression of any other candidate efferocytosis genes. **o**–**r**, Additional quantitative analyses reveals that anti-CD47 antibody has no effect on *in vivo* neutrophil content (as assessed by $Ly6G^+$ area normalized to lesion size) (**o**); macrophage content (as assessed by $Mac\text{-}3^+$ area normalized to lesion size) (**p**); T-cell content (as assessed by $CD3^+$ area across the lesion and adventitia) (**q**); or smooth muscle cell content (as quantified by $\alpha\text{-}SMA^+$ area in the aortic sinus from the external elastic lamina to the lumen) (**r**). **s**, **t**, Anti-CD47 antibody also had no effect on lipid level (s) or serum insulin (**t**). **u**, MTT assays reveal that anti-CD47 antibody has no effect on the proliferation of primary aortic SMCs obtained from $apoE^{-/-}$ mice either at baseline (left) or in the presence of 10% serum (right). Comparisons made by two-tailed *t*-tests, unless otherwise specified. $^{***}P < 0.001$, $^{**}P < 0.01$, $^{*}P < 0.05$. Error bars represent the s.e.m. For gel source data, see Supplementary Fig. 1; for detailed serological data, see Extended Data Table 1. Original magnification, ×4.

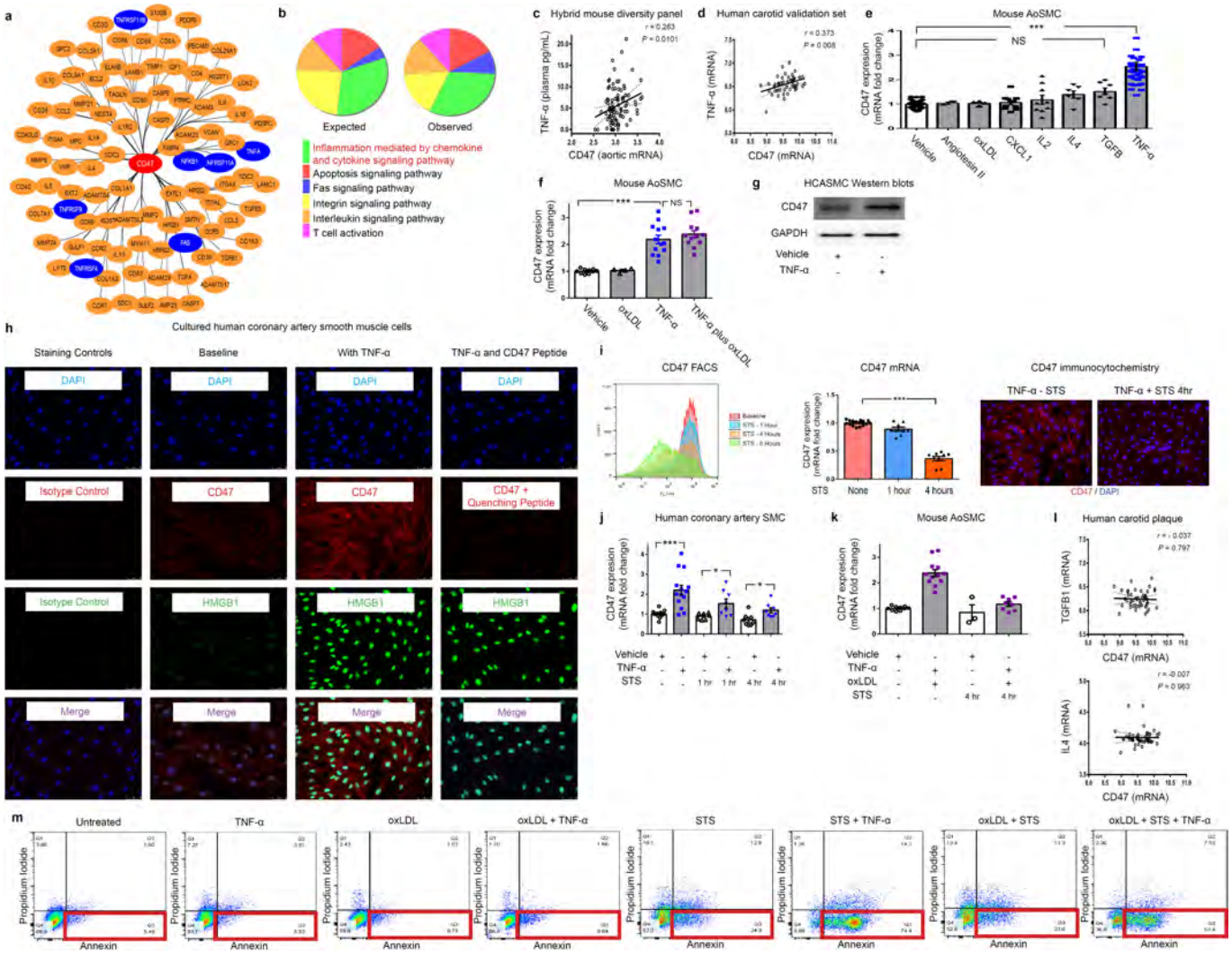

Extended Data Figure 7 | Additional bioinformatic and experimental analyses further implicate a central role for TNF-α in vascular CD47 signalling. a, Cytoscape network visualization of the genes which are significantly correlated with CD47 expression in both human and murine atherosclerotic plaque reveals a high number of TNF-α-related factors (indicated in blue), including ligands, receptors, and downstream signalling factors. **b**, PANTHER pathway analysis of those genes which were significantly associated with CD47 expression in mouse and human vascular tissue and have been previously associated with atherosclerosis through the STAGE study[31], identifies 'inflammation mediated by chemokine and cytokine signaling pathway' as the most over-abundant pathway associated with CD47 expression in vascular tissue. **c**, Using the Hybrid Mouse Diversity Panel (HMDP), which correlates aortic gene expression with Luminex cytokine array data of plasma samples from over 100 inbred strains of mice, we found that vascular CD47 expression is positively correlated with three inflammatory cytokines *in vivo*, including TNF-α, IL-2 and CXCL1. Correlation data shown for CD47 and TNF-α. **d**, Co-expression studies confirm that TNF-α and CD47 expression are positively correlated in human carotid endarterectomy samples from the BiKE validation study. The Pearson correlation coefficient was determined assuming a Gaussian distribution and *P* values were determined using a two-tailed test. **e**, Experiments with primarily cultured mouse aortic SMCs indicate that TNF-α reproducibly induces *Cd47* mRNA upregulation, whereas a number of other classical pro-atherosclerotic stimuli have no significant effect. Notably, CXCL1, IL4, TGF-β and IL-2 fail to induce CD47 expression *in vitro*, as assessed by ANOVA. **f**, Additional studies suggest that the effect of TNF-α on CD47 expression persists in the presence of oxLDL, as occurs in the atherosclerotic plaque. **g**, Western blotting confirms that TNF-α induces CD47 expression in vascular cells at the protein level. For gel source data, see Supplementary Fig. 1. **h**, Immunocytochemistry studies of HCASMCs confirm that CD47 expression is induced on the cell surface of TNF-α treated cells. TNF-α effect is assessed by co-staining for HMGB1, and antibody specificity is confirmed with isotype control and recombinant CD47 peptide quenching assays. **i**, Multiple assays (including FACS, TaqMan and immunocytochemistry studies) reveal that CD47 expression is downregulated on vascular SMCs during programmed cell death, as has previously been observed with inflammatory cells. **j**, Confirmatory assays in cultured human coronary artery SMCs reveal that TNF-α induces changes similar to those observed in murine cells (Fig. 3d), including an induction of CD47 under physiological conditions and a blunting of its expected downregulation during apoptosis. Original magnification, ×20. **k**, The capacity of TNF-α to impair CD47 downregulation during programmed cell death is also observed in mouse SMCs simultaneously exposed to pro-apoptotic stimuli and oxLDL. **l**, No correlation between CD47 and other candidate cytokines was observed in the BiKE biobank, further supporting a specific relationship between CD47 and TNF-α. **m**, Representative FACS-based apoptosis panels from cells exposed to the conditions used in Fig. 3g confirm that TNF-α suppresses efferocytosis (Fig. 3g) despite increasing programmed cell death. Comparisons made by two-tailed *t*-tests, unless otherwise specified. $***P < 0.001$, $*P < 0.05$. Error bars represent the s.e.m.

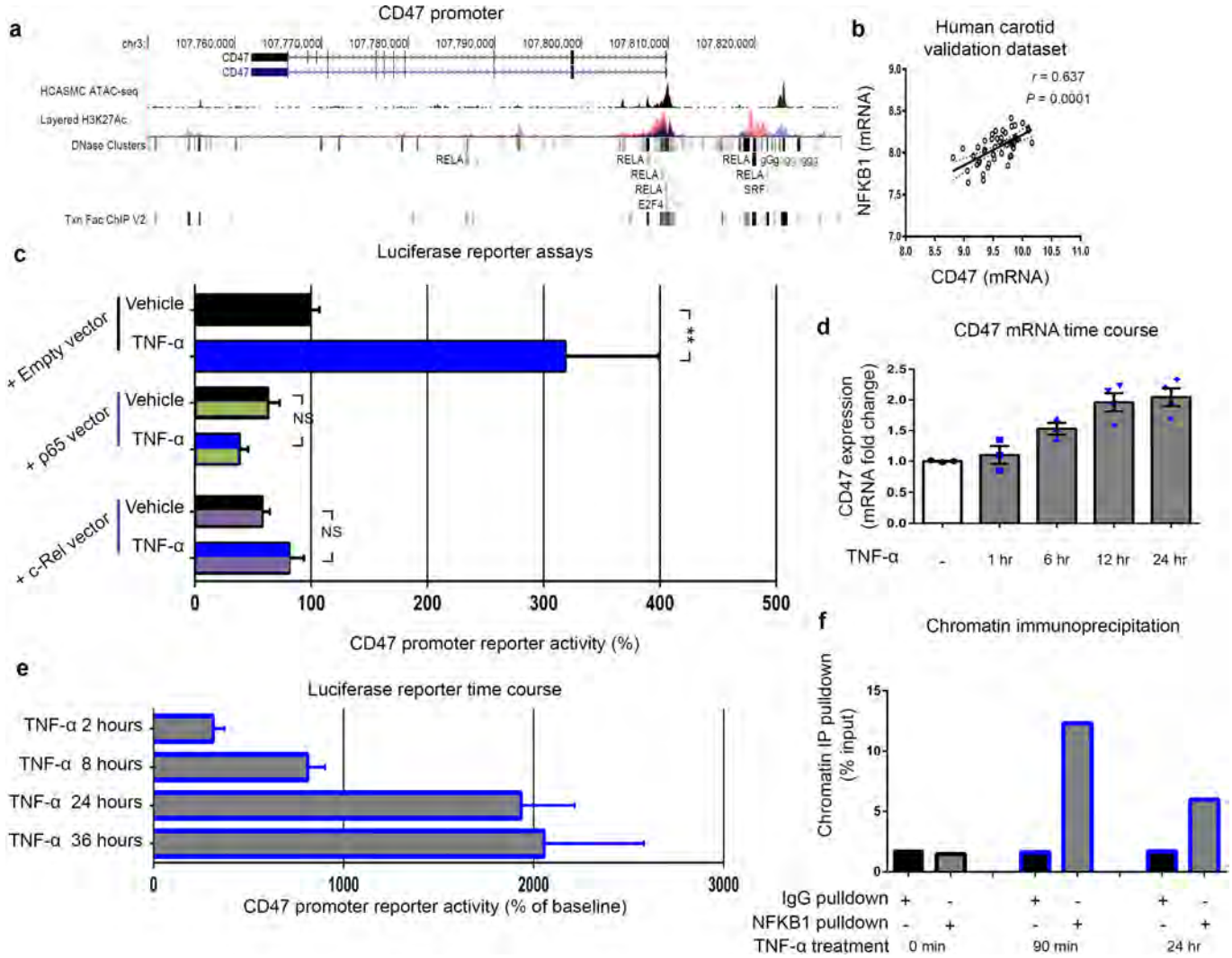

Extended Data Figure 8 | The *CD47* promoter contains predicted binding sites for the TNF-α-related transcription factor NF-κB1. **a**, UCSC genome browser screenshot showing overlay of human *CD47* transcript with ENCODE transcription factor binding sites (including RELA, E2F4, and SRF), along with the active H3K27ac histone modification ChIP-seq track, and a custom track for chromatin accessibility in HCASMCs using the assay for transposase accessible chromatin followed by sequencing (ATAC-seq). These chromatin, DNase hypersensitivity sites, and published ChIP-seq data suggest that members of the NF-κB family of transcription factors could regulate *CD47* expression in vascular tissue. **b**, Additional co-expression studies in the BiKE validation study confirm that *NFKB1* and *CD47* expression are positively correlated in human carotid endarterectomy samples. The Pearson correlation coefficient was determined assuming a Gaussian distribution and *P* values were determined using a two-tailed test. **c**, Additional luciferase promoter reporter assays reveal that induction of CD47 expression requires the presence of NF-κB1 and cannot be induced by other NF-κB co-factors such as RELA or c-REL. **d**, **e**, Time-course studies confirm that CD47 expression is induced by TNF-α within 24 h, suggesting a direct transcriptional relationship (TaqMan mRNA expression assays (**d**); luciferase reporter assays (**e**)). **f**, Additional chromatin immunoprecipitation studies confirm that NF-κB1 protein binds the *CD47* promoter within 90 min of TNF-α-treatment in human coronary artery SMCs. $^{**}P < 0.01$, $^{*}P < 0.05$. Error bars represent the s.e.m.

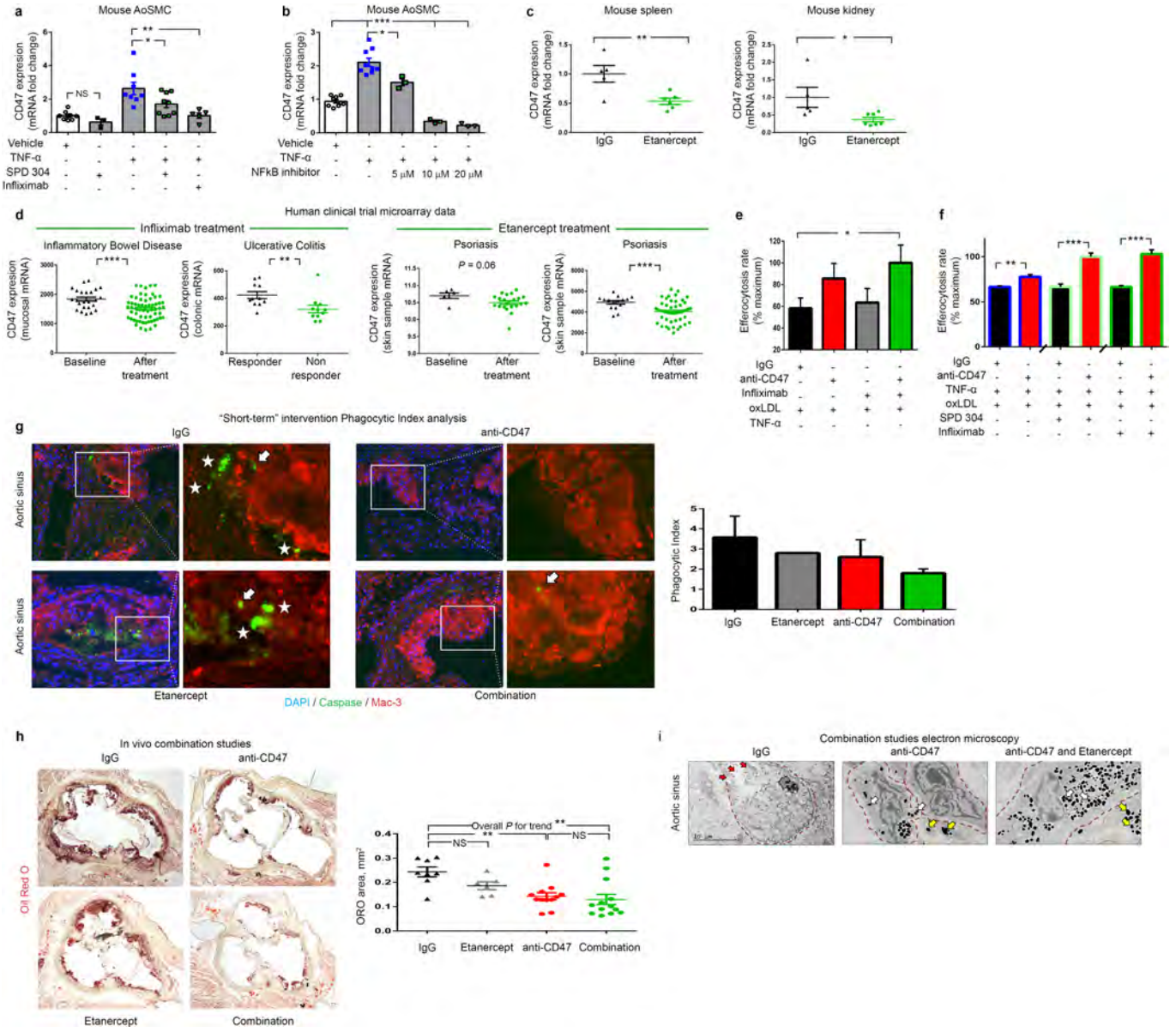

Extended Data Figure 9 | Dual inhibition of CD47 and TNF-α provides a combinatorial effect. a, Pretreatment of mouse vascular SMCs with a chemical inhibitor (SPD 304) or a monoclonal antibody (infliximab) directed against TNF-α prevents the increase in CD47 expression normally seen after TNF-α exposure. **b**, Similar effects were observed with the NF-κB inhibitor, BAY 11-7085, confirming the molecular mechanism outlined in Fig. 4. **c**, Mice injected for four weeks with the decoy TNF-α receptor, etanercept, display a significant reduction in their *in vivo* expression of CD47 in splenic (left) and renal (right) tissue. **d**, Publically available microarray data from human clinical trials of commercially available TNF-α inhibitors reveal that subjects treated with these agents also express lower levels of CD47 *in vivo* (as assessed by two-tailed *t*-tests), confirming the mouse findings above (GSE accession numbers from left to right: 16,879 ($n = 85$), 12,251 ($n = 22$), 47,751 ($n = 28$) and 41,663 ($n = 66$)). **e**, **f**, Additional *in vitro* efferocytosis assays confirm a synergistic effect of anti-CD47 antibodies with a variety of TNF-α inhibitors in both the absence (**e**) and presence (**f**) of exogenous TNF-α. **g**, Mice with established plaques of identical size and with equivalent rates of apoptosis were treated with a short course (5 days) of IgG, anti-CD47 antibodies, etanercept, or combination therapy before collection. As shown the phagocytic index (indicated by the ratio of 'free' (white stars) to 'associated' (white arrows) apoptotic bodies) displayed a non-significant trend towards improvement for combination therapy ($P > 0.05$). **h**, When treated for a full 28 days in the angiotensin-infusion model, individual comparisons showed that etanercept alone had no effect on atherosclerosis, and combination therapy was not significantly different from anti-CD47 alone, probably due to the potent effect of anti-CD47 monotherapy. ANOVA post-hoc test analysis did identify a significant linear trend across all four groups (P for trend < 0.01). **i**, Electron microscopy provides additional qualitative evidence that combination therapy may provide an incremental effect on efferocytosis, as suggested by an increased prevalence of macrophages within the plaque which had ingested a large number of apoptotic bodies (white arrows), a reduced prevalence of free apoptotic bodies (yellow arrows), and a reduced prevalence of uncleared cells undergoing secondary necrosis (red arrows). $^{***}P < 0.001$, $^{**}P < 0.01$, $^{*}P < 0.05$. Error bars represent the s.e.m.

Extended Data Table 1 | *In vivo* serological data and additional *in silico* and bioinformatic data

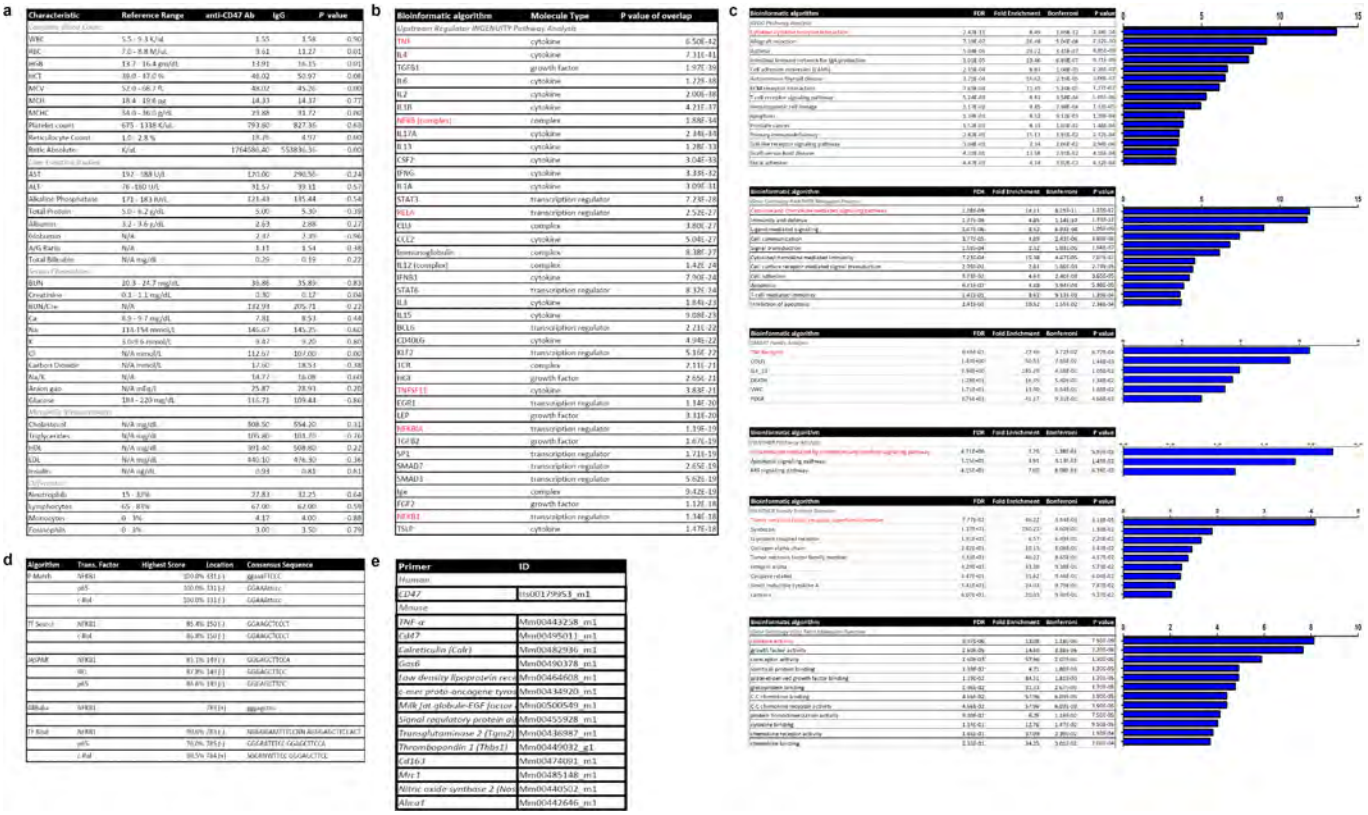

a, Complete serological studies (including blood count, liver function studies, basic metabolic panel and fasting glucose) from the 4-week *apoE*$^{-/-}$–AngII atherosclerosis model indicate that anti-CD47 antibody induces a significant reduction in haemoglobin and compensatory reticulocytosis, consistent with previous reports[4,7]. The erythrophagocytosis of senescent red blood cells appears to be self-limited, and no anaemia was observed in the chronic atherosclerosis model or the reduced dose model ($P = 0.54$ and 0.57, respectively). No significant difference in any other serum marker is observed except for an increase in serum creatinine, which does not deviate outside of the reference range. Metabolic parameters and leukocyte differential data from the 12-week chronic atherosclerosis model are displayed at the bottom of the table. **b**, Additional Upstream Regulator Analysis (URA) bioinformatic analyses of the cytoscape data displayed in Extended Data Fig. 7a performed within the Ingenuity Pathway Analysis (IPA) software identifies a number of TNF-α-related factors (indicated in red) which are predicted to mediate transcriptional regulatory roles in the gene network shown in that panel. *P* values were determined by Fisher's exact test by comparing overlap of co-expressed genes with known upstream regulators from the Ingenuity Knowledge Base. **c**, Several additional DAVID-based bioinformatics analyses including (KEGG, SMART, PANTHER and GO analyses) confirm the association between CD47 and inflammatory signalling related to the TNF-α pathway (indicated in red). Blue panels indicate the $-\log_{10}(P \text{ value})$ for each identified factor. **d**, Transcription factor binding site prediction algorithms identify several putative NF-κB family binding sites within the *CD47* promoter, as displayed in Extended Data Fig. 8a. **e**, List of primers used in this study.